NeuroImage 245 (2021) 118704

Contents lists available at ScienceDirect

NeuroImage

journal homepage: www.elsevier.com/locate/neuroimage

Physical and digital phantoms for validating tractography and assessing artifacts

Ivana Drobnjak[a,1,*], Peter Neher[b,1], Cyril Poupon[c,1], Tabinda Sarwar[d,1]

[a] Center for Medical Image Computing, Department of Computer Science, University College London, UK
[b] Division of Medical Image Computing, German Cancer Research Center (DKFZ), Heidelberg, Germany
[c] BAOBAB, NeuroSpin, Commissariat à l'Energie Atomique, Institut des Sciences du Vivant Frédéric Joliot, Gif-sur-Yvette, France
[d] School of Computing Technologies, RMIT University, Australia

A B S T R A C T

Fiber tractography is widely used to non-invasively map white-matter bundles *in vivo* using diffusion-weighted magnetic resonance imaging (dMRI). As it is the case for all scientific methods, proper validation is a key prerequisite for the successful application of fiber tractography, be it in the area of basic neuroscience or in a clinical setting. It is well-known that the indirect estimation of the fiber tracts from the local diffusion signal is highly ambiguous and extremely challenging. Furthermore, the validation of fiber tractography methods is hampered by the lack of a real ground truth, which is caused by the extremely complex brain microstructure that is not directly observable non-invasively and that is the basis of the huge network of long-range fiber connections in the brain that are the actual target of fiber tractography methods. As a substitute for *in vivo* data with a real ground truth that could be used for validation, a widely and successfully employed approach is the use of synthetic phantoms. In this work, we are providing an overview of the state-of-the-art in the area of physical and digital phantoms, answering the following guiding questions: "What are dMRI phantoms and what are they good for?", "What would the ideal phantom for validation fiber tractography look like?" and "What phantoms, phantom datasets and tools used for their creation are available to the research community?". We will further discuss the limitations and opportunities that come with the use of dMRI phantoms, and what future direction this field of research might take.

1. Introduction

Diffusion-weighted magnetic resonance imaging (dMRI) can non-invasively reveal microstructural features of the brain by exploiting the signal attenuating effect of water molecules diffusing in the tissue. Tractography utilizes the dMRI signal to virtually reconstruct white matter pathways. But the acquired dMRI image undergoes several processing steps (e.g. denoising, motion correction, brain extraction) and local fiber orientation estimation before applying the fiber tractography. Though tractography is a well-established method to study the *in vivo* fiber bundle organization and has found widespread application in the clinical domain and research (Bressler and Menon, 2010; Casey et al., 2005; Ciccarelli et al., 2008; Khundrakpam et al., 2013; Tamnes et al., 2018; Zalesky et al., 2011), it is associated with many challenges and limitations (Jones and Cercignani et al., 2010; Tournier et al., 2011; Maier-Hein et al., 2017a, 2017b).

Many errors can be introduced in the tractography process when inferring the fiber orientation from local water molecules' diffusion profile and tracking these local voxel-wise estimates to reconstruct the continuous streamlines representing structural connections. Moreover, tractography largely also relies on the data quality of the dMRI which is prone to many issues and artifacts including head-motion, low signal-to-noise ratio (SNR), thermal noise, eddy-current artifacts, etc. Regardless of the inherent limitations and challenges of tractography, it remains the only non-invasive method to map connectomes using *in vivo* data (Schilling et al., 2019) to facilitate our understanding of the brain under various conditions of human development and neurological disorders. Hence, with the continuous increase in the utilization of tractography, it is necessary to validate the various algorithms used in the connectome estimation process (Fig. 1) and find the conditions where they succeed and fail.

Any methodological evaluation generally involves comparing against a gold standard, but the absence of the ground-truth for the human brain complicates the evaluation and validation of tractography. The absence of the ground-truth for tractography is referred to as the unavailability of precise local microstructural properties, fiber bundle architectures (crossing, fanning and branching configurations) and global structural connectivity for the human brain. In the context of validation, "phantom" refers to a well-characterized standard that could be used for evaluating the performance or accuracy of MRI methods (Fieremans and Lee, 2018). Conventional methods of tractography evaluation include validating against histological dissection (Hau et al., 2017; Lawes et al., 2008; Stieltjes et al., 2001; Wu et al., 2016; Zemmoura et al., 2014) and tracer findings (Calabrese et al., 2015; Dauguet et al., 2007; Dyrby et al., 2007; Girard et al., 2020; van den Heuvel et al., 2015; Knösche et al.,

* Corresponding author.
E-mail address: i.drobnjak@ucl.ac.uk (I. Drobnjak).
[1] These authors contributed equally to this work.

https://doi.org/10.1016/j.neuroimage.2021.118704.
Received 12 April 2021; Received in revised form 1 October 2021; Accepted 1 November 2021
Available online 6 November 2021.

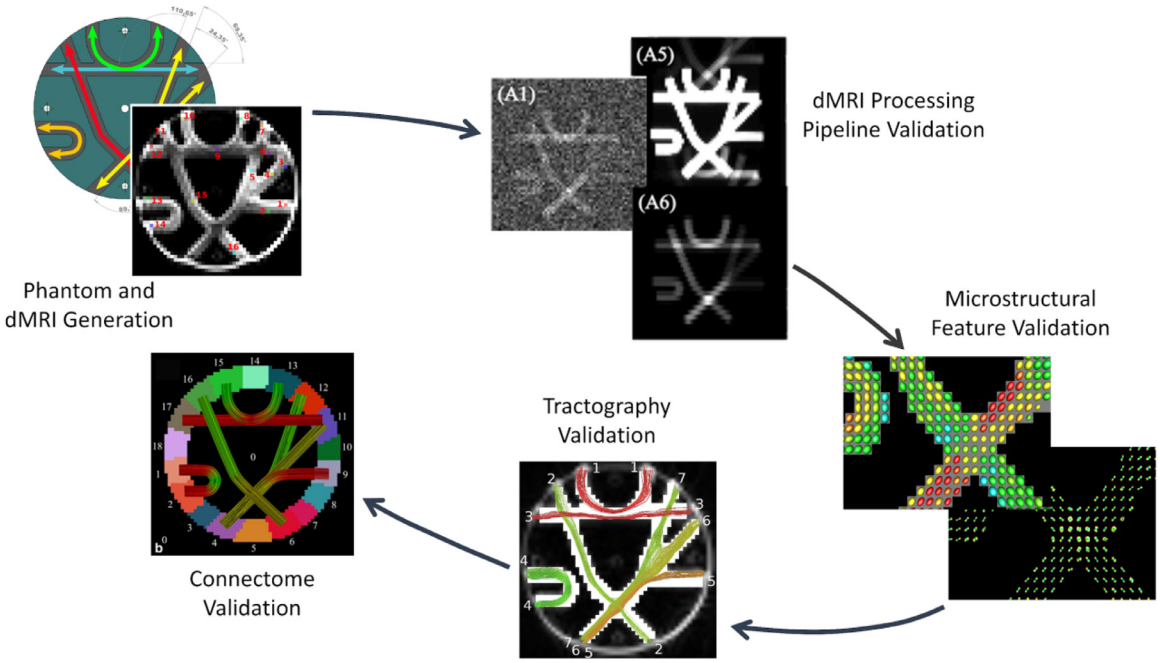

Fig. 1. Overview of the validation process for tractography based connectome estimation. The generated phantom plays an important role as it serves as a ground-truth for the validation process, which could be used to evaluate one or multiple steps involved in mapping connectomes. The generated phantom could be used for evaluating the dMRI processing pipelines (e.g. head motion, noise and eddy-current artifact removal), local microstructural feature estimation, fiber tracts and connectome estimated by tractography. Subfigures adapted from (Côté et al., 2013; Fillard et al., 2011; Neher et al., 2014).

2015; Leergaard et al., 2010). Furthermore, tractography has been validated against circumstantial evidence (Hubbard and Parker, 2009) from functional imaging (Guye et al., 2003; Khalsa et al., 2014; Powell et al., 2006; Skudlarski et al., 2008) and lesion studies (Mori et al., 2002; Newton et al., 2006; Zhan et al., 2015). These conventional methods have provided valuable insights into the performance of tractography algorithms, however generating reference data in the form of phantoms provides control on the generation of the ground-truth and hence can be extremely useful in validating various aspects of tractography (Fig. 1).

Physical phantoms for dMRI research are hardware objects generated using synthetic, natural or glass fibers filled with or soaked in a liquid to approximate restricted diffusion in fibrous tissue. These phantoms undergo dMRI acquisition to generate data that can for example be used to validate fiber tractography. In contrast to physical phantoms that are real world objects, numerical or digital phantoms are virtual objects created using computer simulations providing artificial dMR images as well as a real ground truth for all involved physical and biological aspects (e.g. diameter of the axonal fibers, anisotropic and isotropic diffusivities). Unlike conventional validation methods, physical and digital phantoms offer flexibility and control on the generation of ground-truth that could potentially be used to evaluate various aspects of tractography (e.g. local fiber orientation, geometrical configuration of estimated fiber tracts, control parameters of tractography, etc.).

Phantoms provide precise information of the underlying microstructural properties and hence, serve as validation tools not only to quantitatively and qualitatively evaluate the performance of tractography but also to identify the factors that influence its accuracy. While there are many phantoms in the literature dedicated to validating tractography, the search for the ideal dMRI phantom for the human brain is underway. An ideal phantom is expected to possess the true axonal characteristics, microstructural properties, an ideal model of signal generation, various fiber structures (short, long, deep and superficial fibers) and anatomical connections and true complexity of the human brain (crossing fibers) generated under a wide range of acquisition parameters and artifacts with quantitative quality metrics that could be used for validating the tractography algorithms. Furthermore, it should have realistic magnetic properties such as surface relaxivity (relevant to material wettability) or magnetic susceptibility (relevant to phantom materials). These characteristics are partially satisfied by existing phantoms which will be covered in this review. Though the current phantoms have inherent issues and drawbacks, these serve as a valuable reference system for studying the limitation and accuracy of tractography algorithms.

This manuscript provides an overview of the methodologies, datasets and use-cases of the physical and digital phantoms for validating tractography and artifact removal pipelines. We will discuss the characteristics of these phantoms and how they can serve as potential ground-truth for the validation process. Sections 2 and 3 introduce the two types of phantoms (physical and digital respectively) and the cases where one serves as a better ground-truth than the other will also be discussed along with the gaps between the existing phantoms and the ideal phantom. Sections 2 and 3 also review the tools available for developing the phantoms and the datasets available for evaluating the tractography that can provide the tractography community an opportunity to validate and compare various aspects of the connectome estimation process (Fig. 1). Furthermore, we address the artifacts that could be represented by these phantoms and their potential use for evaluating the dMRI processing pipelines in Section 3. Ideally, these pipelines should remove the artifacts (e.g. thermal noise, eddy-current artifacts) that adversely affect the true water-diffusion signal, restoring the quality and integrity of dMRI data. Section 4 provides the future directions for phantom generation and tractography evaluation based on the limitations and challenges discovered by the validation studies.

Overall, our goal is to provide an overview of the current state-of-the-art phantoms and a guideline for the tractography users on how to use the current phantoms for evaluation purposes along with their associated benefits, challenges, considerations, and limitations. . In this review, we will restrict our discussion to phantoms for validating tractography. The readers are referred to (Fieremans and Lee, 2018) for phantoms to study the brain microstructures with MRI.

2. Physical phantoms

2.1. What are physical dMRI phantoms?

Physical phantoms for diffusion-weighted MRI are objects reproducing the microstructural organization to be found in the cerebral parenchyma whose geometry is perfectly mastered, thus allowing the characterization, testing and validation of biophysical models of the intracerebral water diffusion process as well as of available techniques for inferring anatomical connectivity knowing the ground truth. Physical phantoms are based on the assembly of 4 components: (1) fibres of axon-like geometry to create bundles similar to those found in the brain's white matter, (2) a liquid solution in which the fiber bundles are immersed, (3) a mechanical system to keep the fibres tightly clamped, and (4) a container to ensure the mechanical stability of the fiber bundles.

2.2. Why would you use physical phantoms?

Physical phantoms allow real acquisitions to be made; they are devoid of any hypothesis on the diffusion process in question, unlike digital phantoms which generally use analytical models or Monte-Carlo simulations. In this sense, physical phantoms contribute to obtaining imaging data that integrate both the physical reality of the diffusion process and the artifacts induced during the acquisition process. These artifacts include physical noise, geometric distortions due to eddy currents and field heterogeneities, and intensity bias due to radio frequency heterogeneities. When physical phantoms are designed to preserve their physical properties over time, they can be helpful to tackle the robustness of local models and tractography methods with respect to the MRI instrument. Hence, the variability of the connectomes under imaging devices should be analyzed in isolation from the diffusion model and tractography algorithms. Furthermore, they are useful in multicentre studies to homogenize the diffusion MR imaging protocol in order to control and reduce the variability between imaging devices, but also to perform test-retest studies on the same imaging device in order to check the stability of its tuning over time. In a more general way, tractography physical phantoms can be used for preventive maintenance when acquisitions are carried out on a regular basis with a fixed imaging protocol.

2.3. What variations of physical phantoms are there, what aspects are important?

There are three categories of physical phantoms for tractography validation: isotropic phantoms generally designed for quality control, phantoms dedicated to benchmarking local models made up of a single configuration of fibres (crossing, splitting, kissing), and phantoms dedicated to benchmarking tractography algorithms of more complex geometry and often made up of complex assemblies of fiber bundles. *Ex vivo* biological phantoms can be considered as physical phantoms (Campbell et al., 2006), but this review only focuses on non-biological phantoms combining a liquid solution and a set of microscopically sized solid elements introduced into the solution to act as obstacles mimicking cell membranes (membranes of axonal fibres in this paper).

The process of construction of tractography phantoms involves first braiding of the artificial fiber population in chosen configurations (crossing, splitting, kissing or more complex configurations) and then soaking of those fibers in a liquid/gel. In order for this process to be performed it is important to choose the correct liquid/gel; artificial fibres; the method for braiding; and the method for immersing the fibres into the liquid/gel. We will in this section give an overview of each of these steps.

2.3.1. Nature of the NMR visible component (liquids, gels)

Physical phantoms for the benchmarking of diffusion models and tractography methods are generally based on the use of liquid solutions (including pure water, aqueous solutions, alkanes or mixtures) or gels. The choice of the liquids/gels is crucial since it corresponds to the NMR visible component of the physical phantom, inducing the diffusion-weighted magnetic resonance signal. Its apparent diffusion coefficient is a key characteristic to create phantoms able to mimic the diffusion process occurring in brain tissues and allow the use of the same diffusion imaging protocols as those used *in vivo* in humans.

The simplest diffusion physical phantoms consist of containers filled with a liquid whose viscosity is carefully chosen to match the typical apparent diffusion coefficient (ADC) of the human brain. Pure water is the simplest to use, however, at 20 °C it has a diffusion coefficient of 2.0×10^{-3} mm^2/s, which is much higher than the range of values - measured as ADC - found in the normal white matter ($0.3\text{-}1 \times 10^{-3}$ mm^2/s) (Tofts et al., 2000), and hence is not a good candidate. Ice-water has a much lower diffusion coefficient of about 1×10^{-3} mm^2/s, and has been proposed as a temperature controlled phantom and used in multicenter studies (Chenevert et al., 2011). Alkanes (dodecane or tridecane) could be used since their viscosity can induce a wide variety of apparent diffusion coefficients (between 0.36×10^{-3} and 2.20×10^{-3} mm^2/s at 22 °C), much closer to the average diffusivity observed in brain tissue. But their toxicity can be an issue and their multi resonance spectra causing chemical shifts is not compatible with the use of echoplanar k-space sampling trajectories. As suggested in Keenan et al. (2018a, 2018b), the use of polyvinylpyrolidone (PVP) solutions is indicated and here temperature provides a good way for calibrating diffusivity. A thorough overview of other liquids, water solutions and mixtures can be found in Table 1 in Fieremans and Lee (2018).

Gels have higher viscosity than water resulting in less motion and higher similarity to biological tissues (please see (Fieremans and Deene, 2020) for a complete review). The stability of gels over time must be guaranteed, which is not always the case. A good example of commonly used but unstable gel is agarose which is prone to bacteriological attacks that damage it in the long term. A solution to this issue is the addition of a small quantity of sodium azide to inhibit the growth of bacteria and thus reduce the risk of long-term putrefaction. However, the azide solution is carcinogenic and should therefore be handled with special care. Many alternatives to agarose gel exist (Hellerbach et al., 2013), such as food gels (gelatine, carrageenan, alginate, xanthan gum) or polymers (sodium carbomer, polyacrylic acids, polyvinyl alcohol). One serious drawback of gels is that their high viscosity prevents complex, highly dense, fiber configurations from being fully immersed, and hence liquids are used much more readily.

Magnetic properties of the liquids/gels should also be tuned to match those of brain tissues in order to be able to use diffusion-weighted PGSE sequences with echo times and repetition times similar to that of standard *in vivo* imaging protocols. Gadolinium chelates and manganese chloride are usual contrast agents to modify the T1 and T2 relaxation times (D'Arceuil et al., 2007; Pan et al., 2011). The T1 and T2 relaxation times also depend on the static field B0 and must therefore be calibrated differently for 1.5T, 3T or 7T MRI instruments. Diffusion coefficients depend on temperature, and contrary to *in vivo* tissue whose temperature is naturally regulated, it is important to measure the phantom temperature during each acquisition in order to be able to take into account its variations *a posteriori*. This is particularly the case for ice-water phantoms. Finally, it must be checked that the spectrum of the adopted solution has only one resonance mode in order to avoid ghosting resulting from the superimposition of images at various resonance frequencies in the excitation bandwidth, which is unfortunately the case for many liquids including alkanes and sucrose solutions. For an in-depth discussion of magnetic properties of the diffusion phantoms please see Fieremans and Lee (2018).

2.3.2. Type of matter used to create artificial fibers and beyond; are they similar to that of brain tissues?

In practice, the choice of artificial fibres is mainly guided by their mechanical, magnetic and surface properties in order to make them similar to white matter bundles.

Within the white matter, there is a great diversity in the shape and size of axonal fiber bundles. For example, the projection bundles are very long, have a low curvature and have a large cross-section like the cortico-spinal bundle. In contrast, the U-shaped subcortical association bundles are only a few centimetres long, have a very strong curvature when they follow the shape of the bottom of a sulcus to connect its two sides, and have a much smaller cross-section. Furthermore, a fiber diameter can vary from a few tenths to about ten micrometres, with most axons within the range of 0.1–3.0 μm (Aboitiz et al., 1992; Liewald et al., 2014; Sepehrband et al., 2016). Creating artificial fibres at this scale is extremely challenging. An additional constraint is that the diffusion time is on a clinical scanner typically up to 50 ms, and hence the upper bound for fiber diameter is approximately 10 μm (Fieremans and Lee, 2018). This great variability in shape and size, combined with dimensions limits and sub-micron scales, complicates the construction of realistic phantoms of brain connectivity.

Glass and plastic capillaries were the first to be proposed to design artificial fiber crossings and to simulate the diffusion spectrum (Lin et al., 2003; Tournier et al., 2008). Their inner and outer diameters (50 μm/350 μm) remain out of the range of real axons, thus imposing the use of much stronger diffusion sensitizations and larger diffusion times than conventional imaging protocols. Alternative materials include textile fibres which can be divided into three categories: animal, vegetable and synthetic fibres. Animal fibres (spider silk, sinew, hair, wool) and vegetable fibres (cotton, linen, hemp, rayon) are unfortunately characterised by diameters well over ten micrometres, are brittle, can absorb water (i.e. hydrophilic) and deteriorate with age. They are therefore not suitable for the design of stable physical phantoms.

Synthetic fibres (acrylic, polyamide, polyester, dyneema polyethylene) are more resistant for diameters ranging from 5 to 50 μm and are generally hydrophobic. They are therefore preferred for the design of diffusion MRI physical phantoms (van dem Hagen Elisabeth et al., 2002; Fieremans et al., 2008; Poupon et al., 2008; Lorenz et al., 2008; Reischauer et al., 2009; Moussavi-Biugui et al., 2011a, 2011b; Farrher et al., 2012; Bach et al., 2013; Burcaw et al., 2015; Lemberskiy et al., 2017; Fan et al., 2018a, 2018b). However, care must be taken to ensure that their magnetic susceptibility is close to that of the liquid solution used so as not to induce local variations in the static magnetic field that can bias the diffusion measurements when the fibers are not aligned with the static magnetic field B0. This can be achieved by doping the solution with magnesium chloride to match its susceptibility with that of synthetic fibers (Farrher et al., 2017). fiber bundles made from synthetic fibers induce a sufficient anisotropy profile giving birth to orientation distribution functions (diffusion-ODF) or fiber orientation distributions (fiber-ODF or FOD) whose lobes perfectly match the directions of the underlying fiber populations. These synthetic fibres include the dyneema classically used in the design of ballistic jackets and climbing ropes, which has most of the required characteristics: plasticity, excellent mechanical strength, high degree of hydrophobicity, small external diameter of around 10 μm, magnetic susceptibility, high resistance to chemical attack, high stability over time (Fig. 2).

However, synthetic fibres have a major defect: they are solid fibers and therefore cannot simulate the existence of the two intra- and extra-axonal compartments. In addition, their plain structure drastically reduces the proton density at the voxel level, causing severe SNR issues if the voxel resolution is chosen below a couple of millimeters.

More recently, innovative techniques have been proposed for the creation of hollow fibres. One is the electro-spinning technique which uses two concentric needles connected to the positive and negative poles of a power supply. The process to create hollow fibres rely on a simultaneous injection of solutions of poly-ϵ-caprolactone into the larger diameter needle, and of polyethylene oxide (PEO) into the smaller diameter needle (Hubbard et al., 2015; Zhou et al., 2012) (Fig. 3). Another is the melt-spinning extrusion technique which allows the creation of hollow multifilament polypropylene yarns using a vertical extruder with dedicated spinnerets to design hollow fibers of specific cross-sections (Guise et al., 2016) (Fig. 4).

The choice of injection or extrusion speed allows the internal and external diameters of the fibres created to be accurately controlled in both techniques. Furthermore, since they are automated, they significantly improve the control of the positioning of the hollow fibres and offer the highest anisotropy values.

2.3.3. Technique used to wire the phantom (manual, semi-automatic, fully automatic)

Diffusion MRI physical phantoms proposed in the literature to benchmark tractography algorithms were often unique prototypes, and therefore manufactured using craft processes generally requiring some manual or semi-automated processes. In particular, the achievement of high anisotropy values is conditioned on the one hand by the use of small diameter fibres, but also by maximum compression of the fibres making up the bundles in order to minimize the space left between the fibres and to create highly restricted spaces. While a weak tightening can lead to anisotropy below a level detectable in the presence of acquisition noise, a strong tightening allows anisotropy levels of 0.40–0.60 to be achieved with solid fibres such as dyneema (Fieremans et al., 2008).

There are different strategies for braiding the fiber bundles and ensuring a high level of tightness. The first strategy is based on making negative masks of the bundles that serve as cradles for the fibres (Fig. 5). When done manually, this strategy ensures that the geometry of the outer shell of the fiber bundles is respected (Poupon et al., 2008). The positioning of the fibres in the bundles remains approximate if the braiding operation is carried out manually, and can be improved if it is automated. Fibres are available in the form of large or small locks. In the case of fiber crossings, the locks of fibres belonging to the different bundles can be assembled either bundle by bundle or by alternating the layers of locks corresponding to the different bundles in order to intertwine the fibres. The second strategy is based on the use of heat-shrinkable sleeves that compress fibres previously arranged within the sleeves (Pullens et al., 2010). The geometry of the outer sheath is then less controllable and this second technique does not allow the fibres to be compressed at the crossing points.

2.3.4. Immersion of the diffusion MRI physical phantoms in liquid solutions

Once the fibres have been correctly arranged and tightened by means of a support or heat-shrinkable sleeves, the assembly is placed in a container to be immersed in the chosen target solution. Care should also be taken when filling the container. In order to avoid the creation of air bubbles during the filling process, it is recommended to first de-gas the solution and then fill the container with the solution from its bottom under light vacuum conditions. After filling, the dMRI physical phantom is ultimately sonicated to destroy remaining air bubbles that might have been captured inside the fiber bundles (Fig. 6).

2.4. What available tools/phantoms are there and how are they used?

In the following we will provide an overview over some of the phantoms used for fiber tractography validation and connectomics.

HQ Imaging (http://hq-imaging.com/q-ball-crossing-phantom) offers several products including a phantom called "Q-ball-Crossing-Phantom" made of synthetic fibres and available for different fiber configurations crossing at different angles of 45, 60 or 90° and with 2 possible fiber configurations (Moussavi-Biugui et al., 2011) (Fig. 7):

- interleaved fiber strands for which the two fiber strands are interleaved by alternating winding into the cutouts during the manufacturing,
- stacked fiber strand for which the fiber strands are wound after each other into the cutouts yielding so that they touch each other.

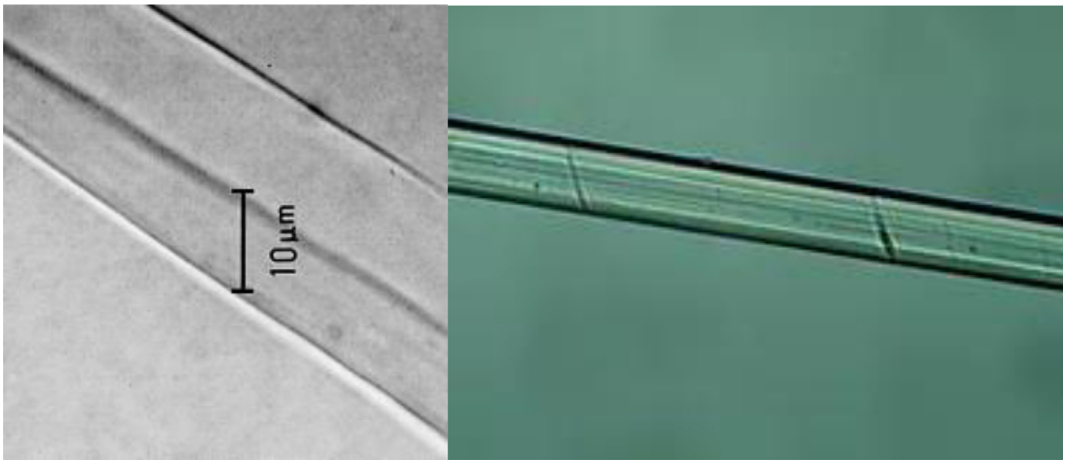

Fig. 2. example of synthetic fibres; (left) acrylic fiber of diameter 20 μm; (right) dyneema fiber of diameter 10 μm. Reproduced from https://www.irbpty.com/dyneema-sk78-and-sk99–1.

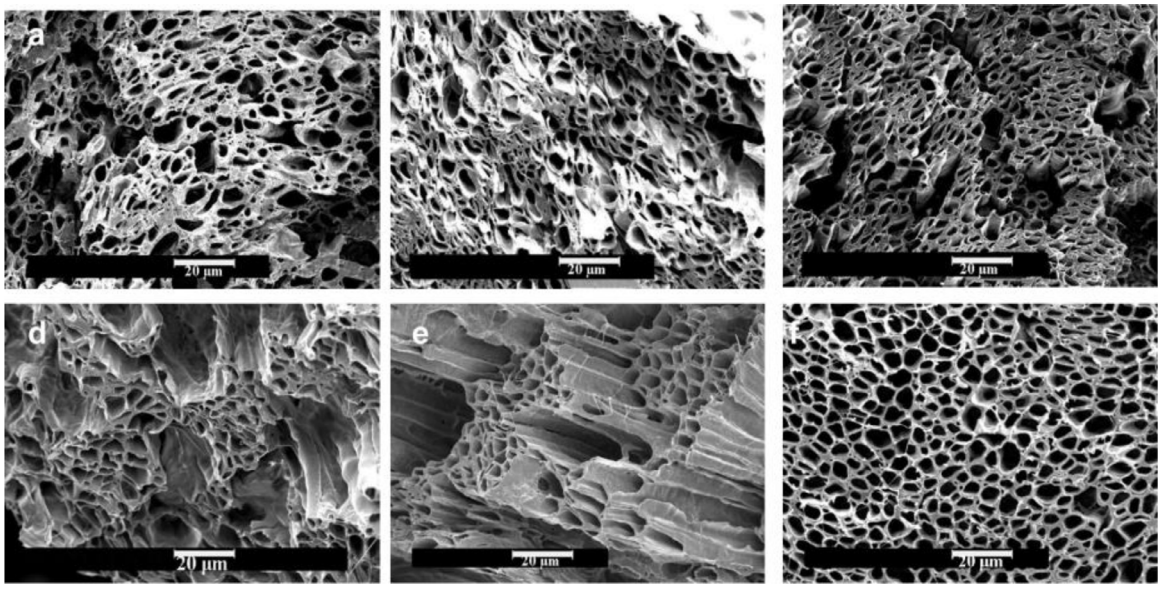

Fig. 3. Electro-spinning: Example of electrospun hollow fibers with different inner diameters according to the process flow. Reproduced from Hubbard et al. (2015).

The “Fiber Cup phantom” was built to meet the needs of the "Fiber Cup" tractography challenge held in London in the frame of the MICCAI conference. This physical phantom was designed at NeuroSpin made from 17 μm diameter acrylic fibres immersed in pure water (Fillard et al., 2011). It mimics a coronal section of a human brain, depicts both long deep and superficial U-fiber bundles and embeds various complex fiber configurations including 2 crossings at 90° and 69.35°, 2 splittings at 45° and 24.35°, 1 kissing between a rectilinear fiber bundle and a semi-circular fiber bundle (Fig. 8). The fiber density was close to 1900 fibres/mm^2. Diffusion MRI dataset were acquired using a Tim Trio 3T MRI system (Siemens, Erlangen) and made available at various spatial resolutions (3 and 6 mm isotropic) and b-values (600, 1500 and 2000 s/mm^2). Competitors were invited to submit their application to the Challenge, and 10 teams provided their results from which a first qualitative and quantitative evaluation of the tractography methods was achieved, showing the superiority of global tractography and advanced HARDI models over streamline tractography algorithms with single tensor estimation. The original diffusion MRI dataset of the FiberCup phantom can be downloaded from the tractometer website.[1] A digital version of the Fiber Cup phantom also exists that was designed using the FiberFox tool, described later in the manuscript that is available from the NITRC website.[2]

The Pullen Crossing Phantom includes X-shaped phantoms each composed of polyester yarn material being itself composed of 18 filaments (“fibers”) with a diameter of 10 μm (Pullens et al., 2010). Twenty-five bundles of 400 yarns (7200 fibers) were interdigitated to form crossings at 30°, 50° and 65° (Fig. 9). Each leg was then tightly maintained using a 14 mm diameter heat-shrinkable sleeve and each crossing was maintained using a 20 mm diameter heat-shrinkable sleeve. After shrinking, the diameter of each leg was reduced to 5.9 mm, and the size of the crossing reduced to 9.3 mm, resulting in a high density of around 8500 fibers/mm^2. The fiber bundles are then immersed in a solution of de-mineralized water doped with manganese chloride to adjust T2 to a value comparable to human white matter T2 and sodium chloride for resistive coil loading. The phantom was used to qualitatively evaluate DTI fiber tracking along with Q-ball and DOT (Diffusion Orientation Transform) reconstructions.

[1] http://www.tractometer.org/original_fibercup/.

[2] https://www.nitrc.org/projects/diffusion-data.

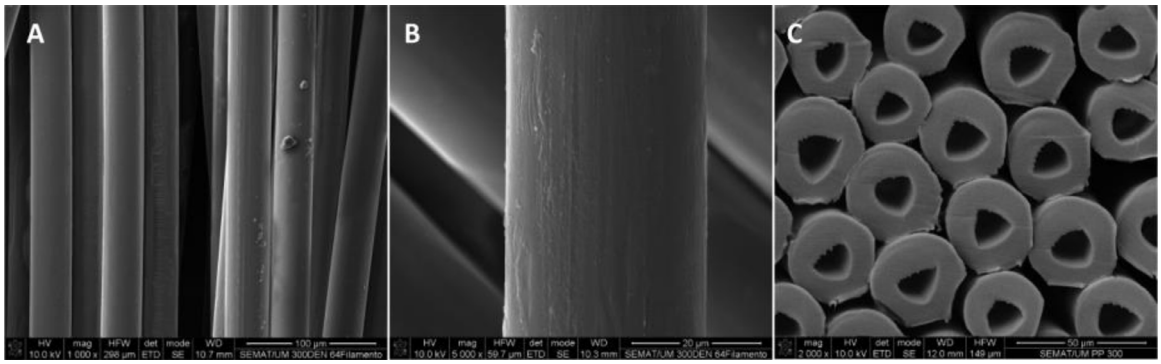

Fig. 4. Melt-spinning: Hollow Polypropylene Yarns of inner diameter 12 μm and outer diameter 34 μm obtained by melt-spinning extrusion. Reproduced from (Guise et al., 2016).

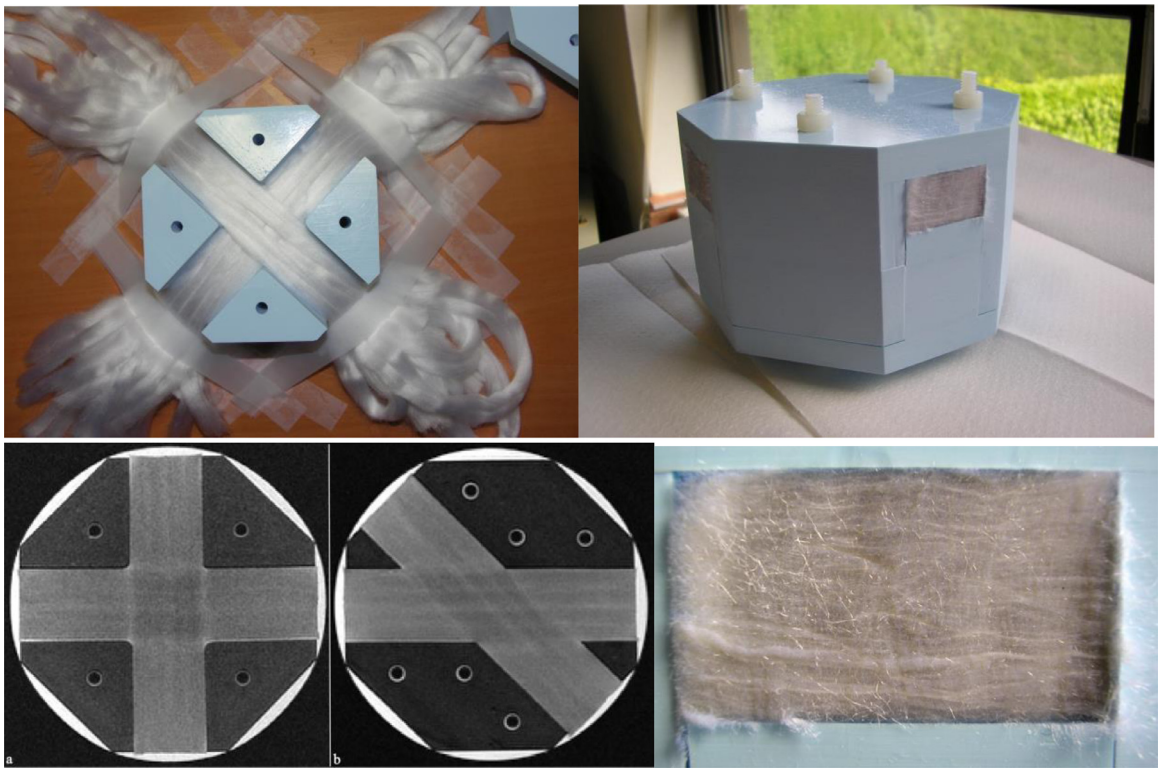

Fig. 5. example of 90° and 45° physical phantoms resulting from a manual wiring of acrylic fibers (outer diameter of 17 μm) inside a container incorporating the negative mask of the target fiber bundles (Reproduced from Poupon et al., 2008).

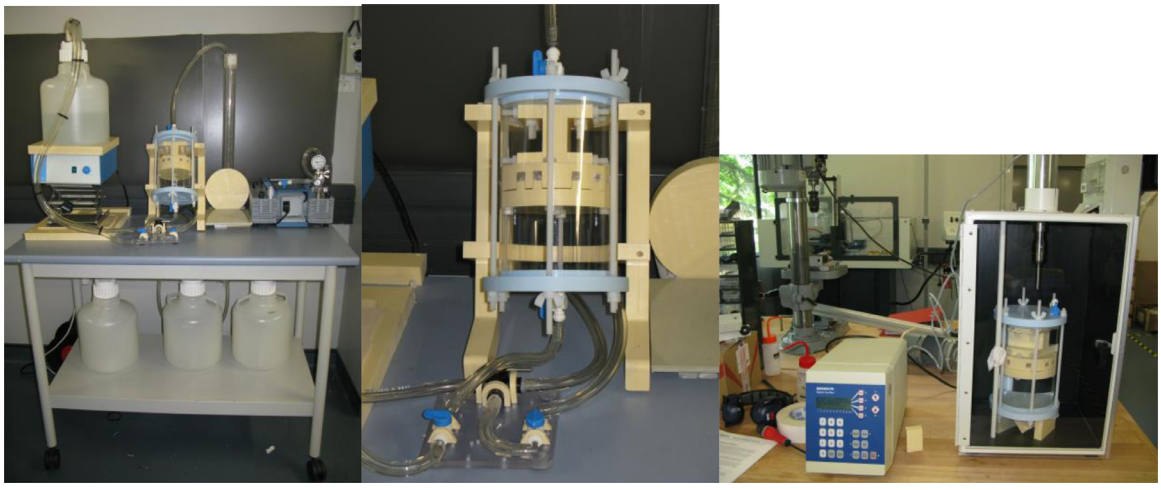

Fig. 6. Filling of a diffusion MRI tractography phantom under vacuum conditions and post-sonication to avoid the presence of air bubbles inside the fiber bundles.

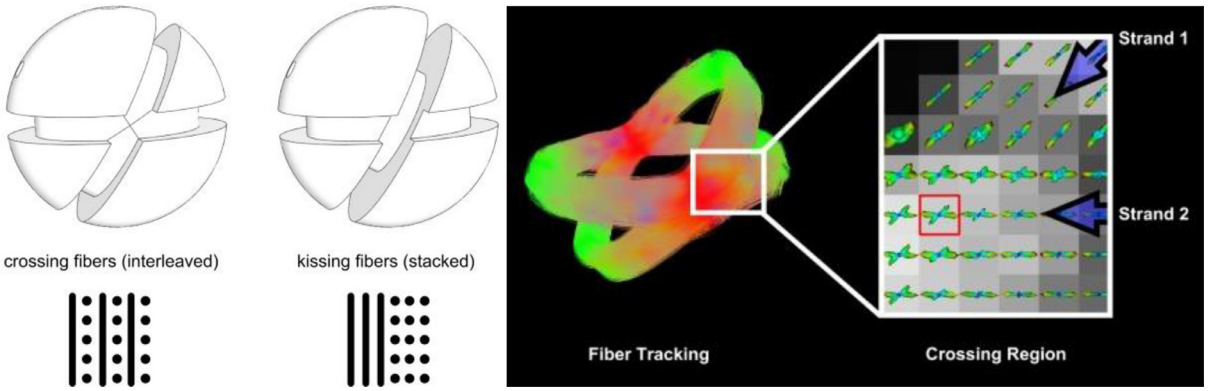

Fig. 7. HQ Imaging Q-ball crossing phantom. Reproduced from http://hq-imaging.com/q-ball-crossing-phantom.

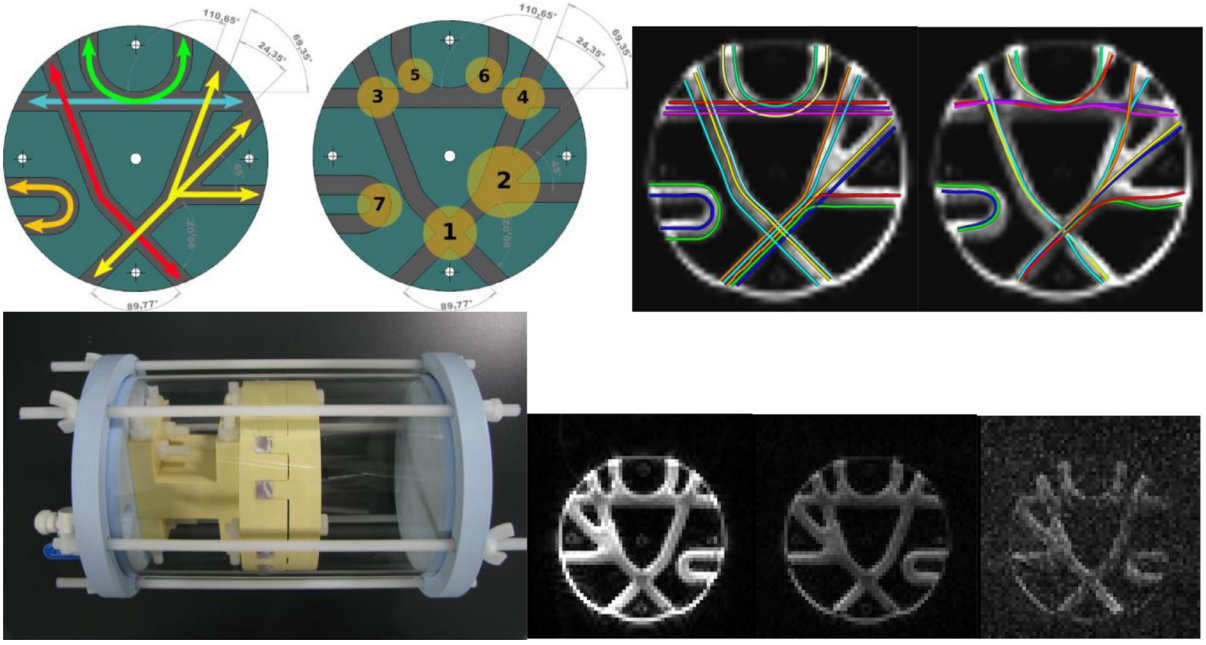

Fig. 8. Fiber Cup dMRI Phantom: (top-left) details of the phantom geometry; (top-right) representation of the various bundle trajectories and results stemming from the best method, e.g. global tractography (Reisert et al., 2011); (bottom-left) phantom filled with distilled water inside its plexiglass container; (bottom-right) dMRI dataset acquired on a 3T MRI system a $b = 0/650/1500 s/mm^2$. Reproduced from Fillard et al. (2011).

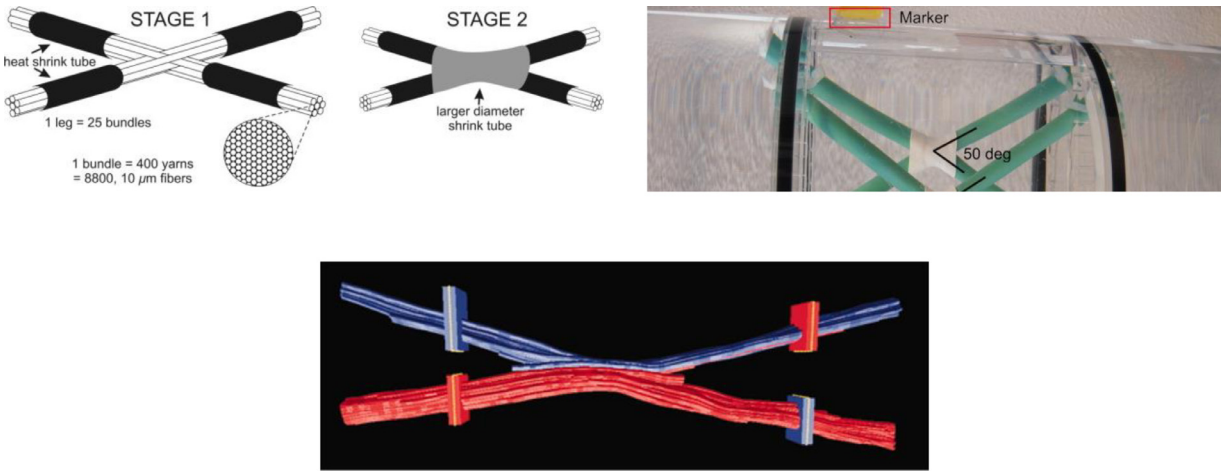

Fig. 9. Pullen Polyester Yarn Phantom: (top-left) details of the X-shaped phantom design from interdigitated hollow yarns; (right) picture of the phantom after shrinking and immersion in water; (bottom-left) 3D rendering of the tractography experiments conducted from the 30° crossing phantom. Reproduced from Pullens et al. (2010).

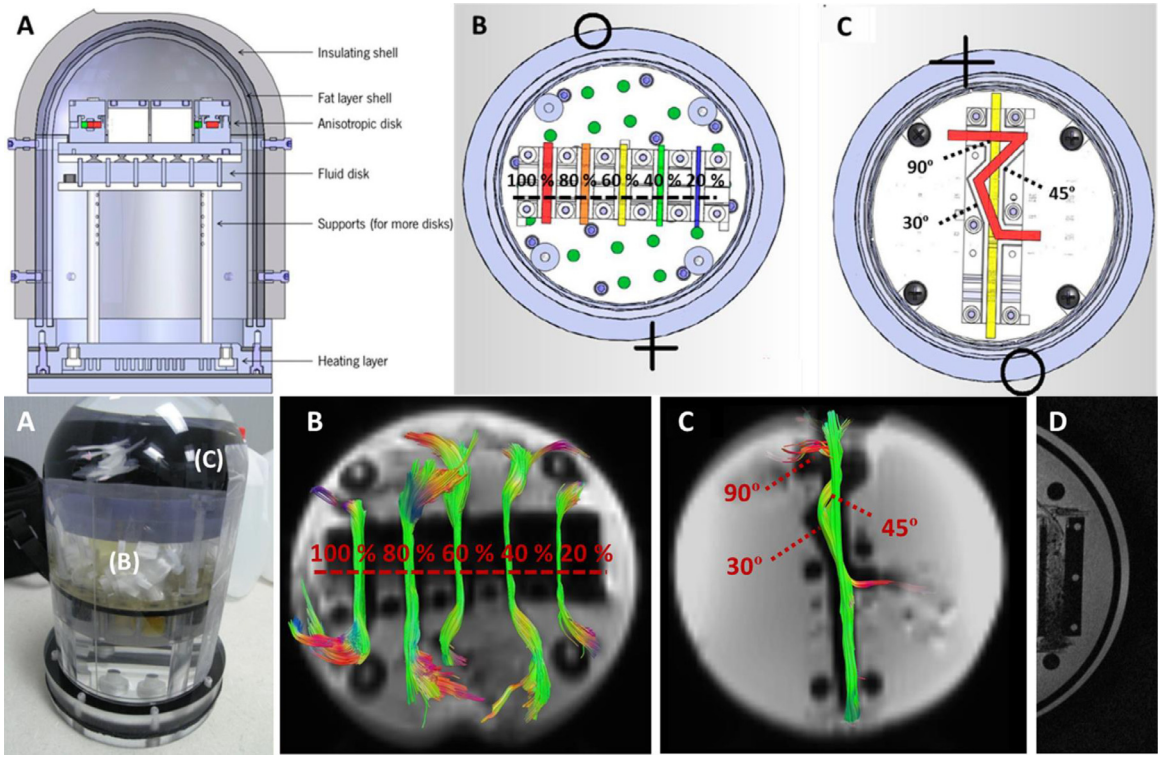

Fig. 10. Guise Hollow Propylene Yarn Phantom: (top) details of the phantom geometry showing 2 frames with various fiber crossings and yarn densities; (bottom) picture of the phantom and 3D rendering of the tractography experiments conducted from the 2 frames Reproduced from Guise et al. (2016).

The Guise Phantom includes a series of disks integrating fiber bundles composed of hollow propylene yarns with various configurations (Guise et al., 2016). In its current release, the physical phantom has 2 disks: one frame with yarns assembled with different crossing angles at 30˚, 45˚ and 90˚ and one frame with bundles depicting different yarn densities at 20%, 40%, 60% and 100% (Fig. 10). This phantom was used to validate High-Definition Fiber Tractography.

A similar phantom was recently used to show that the use of high amplitude gradients (300 mT/m) achievable on the MGH Connectome scanner could measure the internal diameter of the fibers more accurately than a more standard MRI with gradients that could not exceed 80 mT/m (Fan et al., 2018a, 2018b).

Several phantoms composed of hollow electrospun fibres were designed using the electro-spinning technique described earlier (Grech-Sollars et al., 2018; Huang et al., 2021; Hubbard et al., 2015; Ye et al., 2014; Zhou et al., 2021, 2018, 2012) to mimic various axons with different inner diameters and angular dispersions . The various biomimetic neural fiber phantoms were immersed in a solution of cyclohexane and scanned using high field preclinical MRI systems at high *b*-values (>5000 s/mm^2). More recently, there has been a number of follow-up studies focusing on the stability/reproducibility of co-electrospun axon phantom (Grech-Sollars et al., 2018), hydrophilic modification of axon phantom (Zhou et al., 2018), novel co-polymers for axon phantom (Zhou et al., 2021) and the use of brain phantom for validation of microstructural models (Huang et al., 2021).

Watanabe et al. (2006) proposed phantoms with parallel synthetic fibers along with curved and branched patterns to model the complex configuration of WM fiber bundles. Phantoms with four kinds of textile fiber immersed in water were manufactured, which included cotton sewing yarn, monofilament nylon, rayon stitch yarn, and polyester sewing yarn. Lorenz et al. (2008) also manufactured multiple phantoms with five different types of fibers (hemp, linen, viscose, polyamide and dyneema) to model parallel, crossing and bending geometries. The aforementioned phantoms were used to validate tensor tractography. Recent phantoms used 3D printing material to mimic the WM architecture for dMRI (Abu-Sardanah et al., 2018; Mushtaha et al., 2021).

3. Digital phantoms

3.1. What are digital dMRI phantoms?

As described in Section 2, physical phantoms in the context of this article are actual real world objects that can be imaged in an MR scanner. A digital dMRI phantom is the computer generated analogon of a physical phantom, i.e. it is a simulated approximation of a real world object that can be used to study (water-)diffusion effects in a substrate. In contrast to a physical phantom, such a digital phantom typically consists of multiple linked components: (1) a structural model defining the simulated tissue, e.g. the cell shapes and types or the fiber configuration, (2) a diffusion model describing the water diffusion in the structural model that determines the signal attenuation in the diffusion-weighted signal, and (3) some sort of algorithm that enables the simulation of MRI signals and/or images on the basis of the other two components. Depending on who you talk to, probably the signals or images that are simulated using these components are also denoted “phantom”.

3.2. Why would you use digital phantoms?

Each type of phantom, physical or digital, has its own advantages, limitations and correspondingly appropriate use-cases. The most important distinctive feature of digital phantoms is that they are the only way to obtain dMRI data with a real ground truth. Even well defined physical phantoms cannot provide such a perfect ground truth since a direct correspondence between measured signal and component of the phantom is not given and the different aspects that define the phantom itself can only be controlled to a certain extent, e.g. due to mechanical limitations or the statistical nature of the diffusion process. Digital phantoms on the other hand are fully controllable and each aspect of the resulting MR signal can be explained by the phantoms components.

Another important aspect of digital phantoms is that they are relatively easy to manufacture since their creation process does not rely on specialized hardware and raw materials that might be difficult to handle but only on a suitable computation device. Depending on the complexity of the simulation, this enables the cheap creation of large collectives of digital phantom subjects, which are very difficult to reach with other approaches.

Further, digital phantoms are theoretically not constrained in the complexity of their micro- and macro-structural complexity, which is the case for physical phantoms. An increased size and complexity of course comes with an increase in computational cost, potentially requiring supercomputing for high degrees of realism.

3.3. What would the ideal simulated dMRI dataset (for tractography) look like?

As introduced above, phantoms of any kind try to reproduce reality as closely as possible while providing full explainability and controllability. Along this line, an ideal digital dMRI phantom would reproduce the following aspects of reality perfectly: (1) a rich and complex micro- and macro-structure including different cell types and arrangements as well as short- and long-range fiber connections in realistic configurations, (2) diffusion-properties similar to the ones found in the different types of human brain tissue, as well as (3) the actual MR acquisition step including all its effects on the final imaging result.

Due to various reasons, such a perfect reproduction of reality is of course not possible. There are for example computational limitations, i.e. such a perfect simulation involving billions of cells and interacting molecules is simply not calculable with any currently existing supercomputer. Furthermore, even if such massive computations were possible, the resulting simulation would only contain all aspects of what we believe to be an accurate picture of reality. Since our general knowledge about the brain, while constantly increasing, is still limited, this is an intrinsic and currently not resolvable limitation of numerical phantoms. And even under the assumption of complete knowledge about everything there is to know about the brain in conjunction with unlimited computational power, the design process of a correspondingly complex model comprising all this knowledge would doubtlessly still be extremely challenging.

3.4. What variations of dMRI simulations are there, what aspects are important?

Depending on the use-case, the individual components of a dMRI phantom introduced above play a different role, are variably important, and require a different degree of realism required for the application at hand. The structural model can represent a highly variable geometric complexity, depending on the number of tissue types, the number, structure and constellation of individual fiber bundles, the realism of the fiber endings, and the complexity of the microstructure. The microstructure on the other hand can also consist of multiple cell types and other structures including axons, myelin or synaptic terminals, just to name a few and to give illustrations of different scales of complexity.

Depending on the choice of structural model, different types of models for the diffusion process can be employed. Simple structural models, e.g. only defining the rough macroscopic course of a single fiber bundle, are not suitable to be employed in conjunction with a sophisticated model of the diffusion process, e.g. a Monte Carlo method that requires exact definitions of the individual cell shapes and substrates in every single simulated image voxel. On the other hand, many subsequent analyses probably don't require such a sophisticated and also highly computationally intensive diffusion model that can only be employed in certain constrained settings.

This is similar for the simulation of the MR acquisition where different types of simulations with a different degree of complexity and realism can be chosen, e.g. using a k-space formalism, static equations or Bloch equations (Drobnjak et al., 2010a, 2010b; Neher et al., 2014). In certain scenarios, e.g. to analyze the effects of specific artifacts or other MR effects on the resulting fiber tractography, a simulation of the acquisition is surely necessary, but to which extent the simulation has to replicate the real acquisition process has to be decided for each use-case anew.

In fiber tractography validation, typically the main focus is the macroscopic structure since this directly influences the actual tractography step. In this case, the simulation of the diffusion weighted signal is often performed using simple parametric models, such as the diffusion tensor, and the actual MR acquisition is not simulated at all. The previous steps in the tractography pipeline, namely the image preprocessing and the local tissue modeling are typically analyzed and evaluated independently, since a joint analysis of the complete pipeline leads to a combinatorial explosion and a comprehensive study disentangling the effects of the individual components is difficult to realize. Simulated dMRI phantoms used for analyzing these steps of the tractography pipeline are consequently focusing on the realistic simulation of the actual MRI acquisition and a complex microstructural and diffusion model respectively.

Nevertheless, over the last years, microstructural information became increasingly relevant for some novel tractography approaches, e.g. by Daducci et al. (2015a, 2015b, 2016), and therefore their realistic simulation, including a more sophisticated diffusion model, beyond simple fiber crossings gained importance in the field of tractography. Also, the evaluation of fiber tractography matured to a research field of its own, and more comprehensive simulations for performing validation studies became increasingly relevant, featuring not only a complex macroscopic fiber architecture but also a sophisticated simulation of the diffusion process and of the actual MR acquisition.

3.5. What tools and methods are out there?

In the following we want to provide an overview over some of the methods used for simulating diffusion-weighted MRI phantoms for different purposes, namely fiber tractography, connectomics and artifact correction.

3.5.1. Simulating a diffusion-weighted signal

The simulation of diffusion-weighted signals can be approached on two levels of complexity. The signal is either synthesized using complex Monte Carlo simulations of diffusing molecules in certain well-defined structures (Laun et al., 2009; Grebenkov, 2011; Zhang et al., 2011; Ginsburger et al., 2018, 2019; Palombo et al., 2019; Rafael-Patino et al., 2020) or a parametric diffusion signal model that allows for the analytic calculation of the signal attenuation is employed (Basser et al., 1994; Assaf and Basser, 2005; Zhang et al., 2012; Panagiotaki et al., 2012; Alexander et al., 2019) - for a comprehensive review of both please see (Fieremans and Lee, 2018). Numerical simulations of the diffusion process are computationally challenging and are therefore mainly used to simulate diffusion in a single voxel. The multiple correlation function tool (MCF) (Laun, 2012) and UCL Camino Diffusion MRI Toolkit[3] are two openly available software packages that enable such simulations. Recently, another open-source approach was introduced in Lee et al. (2021) that implements Monte Carlo simulations in 3D voxelized segmentations of cells in microscopy images. These approaches focus on the actual diffusion modeling and are frequently used for the development or evaluation of localized methods, such as signal reconstruction or the analysis of microstructure.

For methods that work on multiple voxels or a whole image simultaneously (e.g. fiber tractography, connectomics or tract-based spatial statistics), an artificial signal in hundreds and thousands of voxels has to be synthesized. To this end, parametric models, which are computationally much more lightweight, are more appropriate and commonly

[3] http://camino.cs.ucl.ac.uk/.

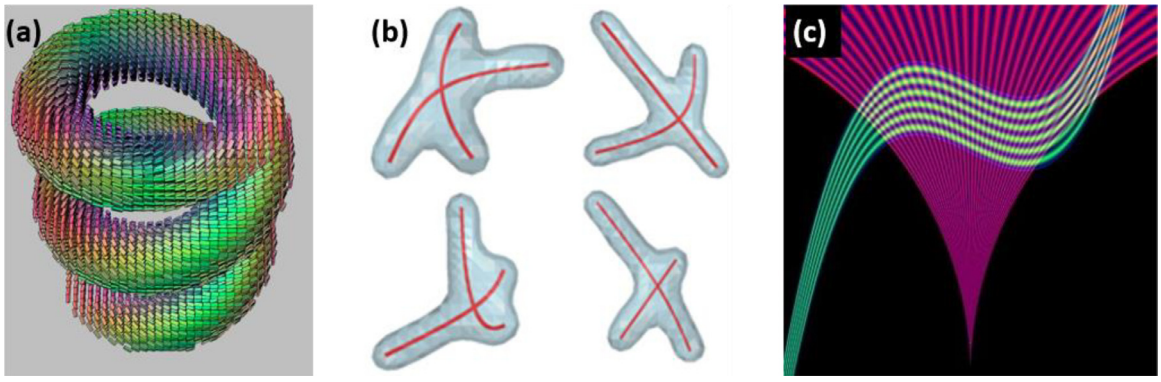

Fig. 11. Anisotropic diffusion tensors (a) generated with the tend helix tool (Teem, 2021), randomized fiber crossings (b) used by Cetingul et al. (2012), and a crossing between two fanning and curved 2D tensor fields (c) used by Aganj et al. (2011). Figures adapted from the respective works.

used. Even though they are based on a quite simple model of the underlying tissue, which is only valid in certain very specific situations, parametric diffusion modeling proved to be very valuable for a large number of tasks. By far the most common way to model an anisotropic diffusion-weighted signal is to employ a prolate tensor model. Furthermore, a large variety of specialized models that characterize the diffusion in different tissue compartments has been introduced over the last years. Commonly, the diffusion process in white matter tissue is partitioned into restricted anisotropic diffusion inside of the axons, hindered anisotropic diffusion between the axons, a restricted compartment modeling the diffusion of water trapped in other cell types and an additional isotropic compartment (Assaf and Basser, 2005; Panagiotaki et al., 2012). To increase the degree of realism most simulations include thermal noise following a Rician distribution, which is correct for single-channel MR acquisitions (Gudbjartsson and Patz, 1995). Furthermore, methods have been developed to simulate diffusion signal for a range of different gradient waveforms, other than Single Diffusion Encoding (SDE), such as Oscillating Gradients, Double Diffusion Encoding and Generalised Waveforms[4] (Drobnjak et al., 2011, 2010a, 2010b; Ianuş et al., 2016, 2013).

3.5.2. Simple simulations for creating white matter fiber phantoms

The most common way to create multi-voxel macroscopic fiber structures suitable for tractography analyses described in the literature is by using mathematical functions that model the course and shape of one or multiple fiber bundles in 2D or 3D. The earliest approaches of this type modelled relatively simple geometric bodies, such as lines, circles, ellipses, helices and fiber crossings or other shapes defined by simple mathematical functions (Gössl et al., 2002; Tournier et al., 2002; Lori et al., 2002, ; Lazar and Alexander, 2003; Kang et al., 2005; Kreher et al., 2005; Staempfli et al., 2006; Batchelor et al., 2006; Aganj et al., 2011; Cetingul et al., 2012; Wu et al., 2012) that define the local anisotropic diffusion, typically embedded in an isotropic non-fiber surrounding. Fig. 11 illustrates examples for this approach.

Typical use-cases of these phantoms are to evaluate the effects of noise, number of averages, voxel size, voxel aspect ratio, data type, stepping algorithm/interpolation, step size, pathway anisotropy and surrounding anisotropy on the outcome of local fiber tractography by assessing the number of prematurely ending tracts (Lazar and Alexander, 2001; Gössl et al., 2002; Chen and Song, 2008), tract dispersion with increasing distance from the seed region (Lazar and Alexander, 2003), the distance to a ground truth tract (Lori et al., 2000, 2002, ; Lazar and Alexander, 2003) or the performance in crossings (Kreher et al., 2005; Staempfli et al., 2006). Many studies only evaluated a single tractography algorithm without comparison with the state of the art; others assessed the performance of streamline algorithms with different integration methods (FACT, Euler, Runge-Kutta) (Lazar and Alexander, 2003) or compared tensorline and streamline approaches (Lazar and Alexander, 2003, 2001). Aganj et al. (2011) used two simulated fanning and crossing 2D fiber bundles (see Fig. 11(c)) to evaluate their global tractography approach based on a 3D Hough transform. Cetingul et al. (2012) used 60 randomized phantoms of two crossing fibers (see Fig. 11(b)) to quantify tractography errors as the symmetrical Chamfer distance between the estimated tract and the ground truth centerline. Advanced simulations for creating white matter fiber phantoms

Over the recent years, the means to create much more complex, variable and realistic macroscopic fiber structures improved a lot and an increasing number of simulation methods were introduced and proved to be very useful for the validation of fiber tractography (Leemans et al., 2005; Delputte et al., 2006; Barbieri et al., 2010; Close et al., 2009; Caruyer et al., 2014; Neher et al., 2014).

Leemans et al. (2005) introduced a mathematical framework for the simulation of complex white matter DTI phantoms. This framework models white matter bundles by generating a set of points defining the tract progression. These points are interpolated using a piecewise differential 3D space curve, yielding an analytic definition of the fiber centerline. By convolving this centerline with a circularly symmetric kernel function the physical extent of the white matter bundle is defined. The kernel function also characterizes a non-constant fiber density within the bundle that depends on the distance to the fiber centerline. To generate the actual signal, a prolate tensor model characterized by a density-dependent FA and MD, embedded into an isotropic background, is used. The principal diffusion direction of the tensor is obtained directly from the fiber centerline. Fig. 12 illustrates the approach. By summing several bundles, configurations like crossings or kissings can be generated.

Delputte et al. (2006) used the approach by Leemans et al. (2005) to generate a synthetic dataset on the basis of a fiber tractogram obtained from a smoothed *in vivo* diffusion-weighted image. Each streamline is treated as a centerline for one synthetic fiber bundle. Additionally they added Rician noise to the resulting dataset and used it to validate fiber tractography methods by calculating the distance between the ground truth fibers and the tractography results. Jeurissen et al. used the framework of Leemans and colleagues to measure tract dispersion of a probabilistic CSD tractography algorithm based on the residual bootstrap as a function of arc length along the trajectory for gold standard (Jeurissen et al., 2011).

A more comprehensive approach to simulate realistic dMRI images of the brain including multiple tissue types was pursued by Barbieri et al. (2010). They used anatomical scans from the BrainWeb

[4] http://mig.cs.ucl.ac.uk/index.php?n=Tutorial.MISST.

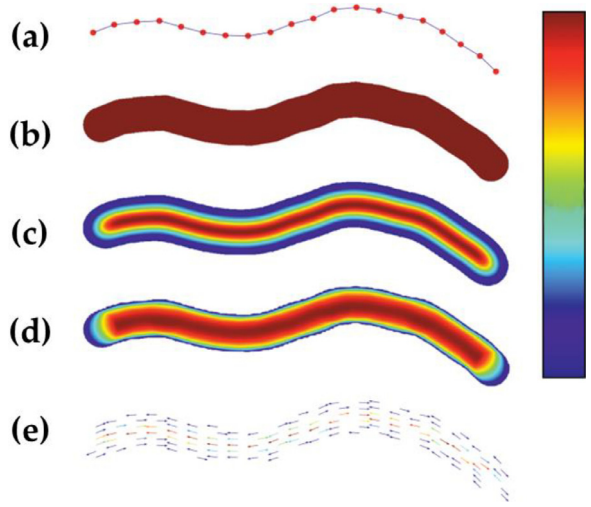

Fig. 12. Illustration of the phantom generation process proposed by Leemans et al. (2005). Definition of the fiber centerline (a), convolution with different kernel functions resulting in varying fiber densities (b–d) and resulting principal directions of the tensor field (e). Figure adapted from Leemans et al. (2005).

project[5] to determine WM, GM and cerebrospinal fluid (CSF) probability maps. The values of these maps were used as input for the simulation of the dMRI signal attenuation using the CHARMED model (Assaf and Basser, 2005). To define the principal directions of the WM compartment model, fiber bundles were defined manually using the approach similar to Leemans et al. (2005). In voxels without such an explicit definition of the local fiber direction, the principal diffusion direction was chosen randomly with an additional smoothness constraint based on the surrounding tissue. Fig. 13 illustrates the resulting tensor maps.

Barbieri et al. were also the first to show the simulation of more complex artifacts than thermal noise in a fiber tractography phantom by adding aliasing and N/2 ghosts. The incurrence of these artifacts was not achieved by simulating the actual physical process but simply by adding intensity scaled and shifted copies of the artifact-free image to itself (see Fig. 14).

Close et al. published an open-source command-line tool called numeric fiber generator (NFG) that generates random fiber structures with a focus on the dense packing of fiber bundles that also occurs *in vivo* (Close et al., 2009). To this end whole bundles are modeled by single thick strands with circular cross-section, which are initialized along straight line segments between randomly generated points on the surface of a sphere. These straight tubes are optimized with respect to a function controlling the overlap between the individual bundles. The parts of the bundles that are pushed outside of the sphere are subsequently removed. In a fourth step, the thus produced bent fiber strands are subdivided into sub-bundles, each represented by a thinner strand that is also modeled as a tube with circular profile. These sub-bundles are again optimized with respect to the same overlap-controlling function as the main bundles. This second optimization step causes the sub-bundles to better adapt to their surroundings, which causes intra-bundle deformations and deviations from the circular profile shape. The whole process is illustrated in Fig. 15. The diffusion-weighted signal is then generated by placing a prolate tensor in each voxel covered by the fiber strands, pointing in the direction of the closest sub-bundle. To simulate regions containing, for example, CSF, spherical exclusion regions can be placed, inside which no fiber bundles are allowed. The diffusion inside of these exclusion regions is modeled with an isotropic tensor. By initially generating the image with a high resolution and successive downsampling, partial volume effects are simulated. Additionally Rician noise can be added to the data. The NFG is openly available on nitrc.[6]

Caruyer et al. (2014) published their Phantomas dMRI simulation tool, which enables the creation of spherical phantoms similar to Close et al. but with some significant differences. The macroscopic structure modelled with Phantomas consists of tubes with constant radius whose course inside a sphere is determined by its center line which in turn is defined by user controllable control-points connected by 3rd order piecewise polynomials. In contrast to Close et al., this approach focuses on the full controllability and not on a dense and automatically optimized fiber structure. Spherical isotropic regions mimic CSF compartments in the brain. Fig. 16 illustrates the macroscopic structure of a Phantomas phantom. The third compartment modelled by Phantomas, gray matter, is defined by the remaining empty space inside the sphere. By overlaying the whole structure with an arbitrary voxel grid, the volume fractions of the individual compartments in each voxel can be calculated. The signal attenuation caused by diffusion effects in WM is computed based on a CHARMED model, where the extra-axonal compartment is modeled by a diffusion tensor and the intra-axonal compartment is modeled by a cylinder using a corresponding template diffusion profile. Phantomas further calculates an approximation of the image contrast changes introduced by compartment specific tissue relaxation with T1 and T2 relaxation times representative for *in vivo* brain tissue. While not simulating the actual MR acquisition with all of its effects, this is the first dMRI phantom tool usable for fiber tractography that simulates relaxation induced contrast changes.

The Phantomas website features a web interface for defining the fiber structure and its source code is available openly on GitHub.[7] Phantomαs was used to create the testing and training data of the 2nd HARDI Reconstruction Challenge,[8] organized at ISBI 2013.

With the Fiberfox dMRI simulator, Neher et al. (2014) presented an approach that unifies many aspects of the previous approaches in one comprehensive tool. Fiberfox simulates diffusion based on a flexible multi-compartment model enabling the simulation of intra- and extra-axonal diffusion as well as CSF and gray matter using various parametric compartment models (stick, tensor, astrostick, ball or dot). The white matter macrostructure is defined by conventional streamlines, as they are produced by most tractography algorithms. This enables the direct usage of realistic tracts in the form of native or curated whole brain tractograms. Additionally, Fiberfox provides functionalities to manually create well defined artificial configurations such as crossing, kissing, twisting or fanning fiber bundles as well as to create random configurations similar in style to the numeric fiber generator by Close et al. (2009). Besides a high flexibility regarding the shape of the individual bundles with a variable cross-section, progression and density, the choice of a white matter model in the form of individual streamlines further enables a rich sub-voxel structure. The non-fiber compartments are defined by classic volume fraction maps.

Fiberfox further simulates the actual k-space acquisition, enabling a straightforward and realistic introduction of MRI effects, such as complex gaussian noise, eddy currents, inter-volume head motion, distortions, spikes, aliasing, N/2 ghosts, signal drift, Gibbs ringing and relaxation. This simulation of the MR acquisition can be controlled by a number of parameters typical for real MR scanners (e.g. TE, TR, partial fourier factor, ETL, readout type, *b*-value and gradient directions) and human tissue in the form of compartment specific relaxation constants (T1, T2) and diffusivities.

Fiberfox is included in the Medical Imaging Interaction Toolkit (MITK) and openly available as source code and binary application.[9] The complete simulation is controllable via a graphical user interface

[5] http://www.bic.mni.mcgill.ca/brainweb/.

[6] http://www.nitrc.org/projects/nfg/.

[7] https://github.com/ecaruyer/phantomas.

[8] http://hardi.epfl.ch/static/events/2013_ISBI/.

[9] https://github.com/MIC-DKFZ/MITK-Diffusion/

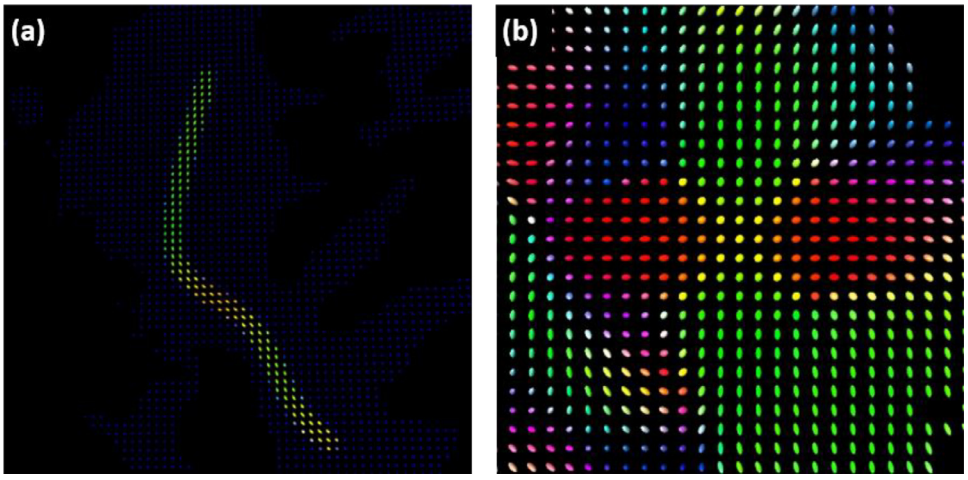

Fig. 13. Illustration of the DTI phantom proposed by Barbieri et al. (2010). (a) shows a white matter strand embedded into a homogeneous background. (b) shows the tensor image resulting from two crossing fiber strands embedded into a background signal with smoothly changing random orientation. Figure adapted from Barbieri et al. (2010).

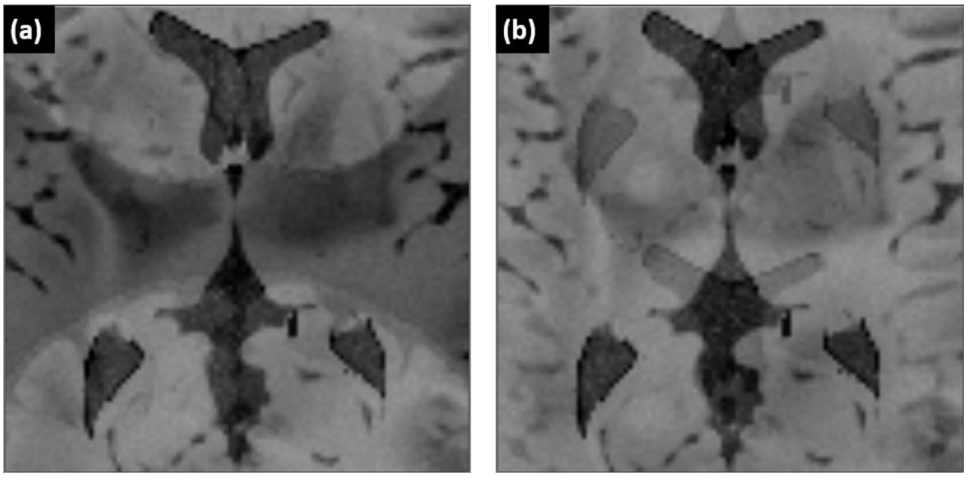

Fig. 14. Barbieri et al. (2010) simulated aliasing (a) and ghosting (b) artifacts by adding intensity scaled and shifted copies of the artifact free image to itself. Figure adapted from Barbieri et al. (2010).

as well as batch-processing-friendly command line application. Multiple datasets generated with Fiberfox and usable for fiber tractography validation have been published and are openly available (Neher et al., 2014, 2017b; Maier-Hein et al., 2015, 2017a, 2017b; Neher and Maier-Hein, 2019, 2020a, 2021). The phantom simulated for the ISMRM Tractography Challenge 2015 (Maier-Hein et al., 2017a, 2017b) is now one of the most widely used dMRI phantom datasets in the area of fiber tractography validation (Neher et al., 2017a; Poulin et al., 2017; Théberge et al., 2020; Benou and Riklin Raviv, 2019; Wegmayr et al., 2019). In the context of the challenge it was used to evaluate 96 distinct tractography submissions from 20 research teams using the Tractometer evaluation suite (Côté et al., 2013). Building on the experiences made with this single brain-like phantom, Neher et al. recently published a large dataset of 99 subjects with various realistically simulated image contrasts and variations of acquisition parameters that extends the ISMRM challenge phantom in terms of the number of simulated images and subjects, the structural phantom complexity (71 major white matter tracts) and the range of simulated MRI artifacts. Fig. 17 illustrates some of the phantoms created with Fiberfox.

An approach to manually define artificial fiber bundles similar to Fiberfox with a focus on polarized light imaging but also applicable to dMRI, the FAConstructor, was recently presented by Reuter et al. (2019). FAConstructor is openly available on GitHub.[10] Another approach for simulating dMRI images that is very similar to Fiberfox was presented by the authors of D-BRAIN (Perrone et al., 2016), albeit without the possibility to simulate realistic artifacts.

3.5.3. Simulating connectomic networks

The majority of the described phantoms were developed with a focus on the evaluation of local microstructural features and the geometrical configuration of the fiber bundles reconstructed by tractography. Another aspect of validation focuses only on the evaluation of connectivity estimated by tractography without regarding the shape or course of the underlying bundles that form the connection (Sarwar et al., 2020). The typical considerations for connectome mapping are the presence/absence of a fiber bundle between pairs of regions and the strength of the connecting fibers. For this purpose, Sarwar et al. simulated 2d and 3d connectome phantoms where nodes/regions were positioned on the circumference of the circle and surface of the sphere respectively - Fig. 18(a,b) (Sarwar et al., 2019). The connectivity matrices of these phantoms were simulated using generative models that preserved the topological properties of the human brain, which include degree, betweenness centrality, clustering coefficient, characteristic path length, global efficiency, modularity and interconnectivity between hubs (Betzel et al., 2016). The predefined connections were then modeled as curved tubular fiber bundles of fixed diameter. This connectome phantom generation process is presented in Fig. 18(c). The simulated phantoms were used to compare the binary connectomes estimated by deterministic and probabilistic tractography algorithms. The spher-

[10] https://github.com/3d-pli/FAConstructor

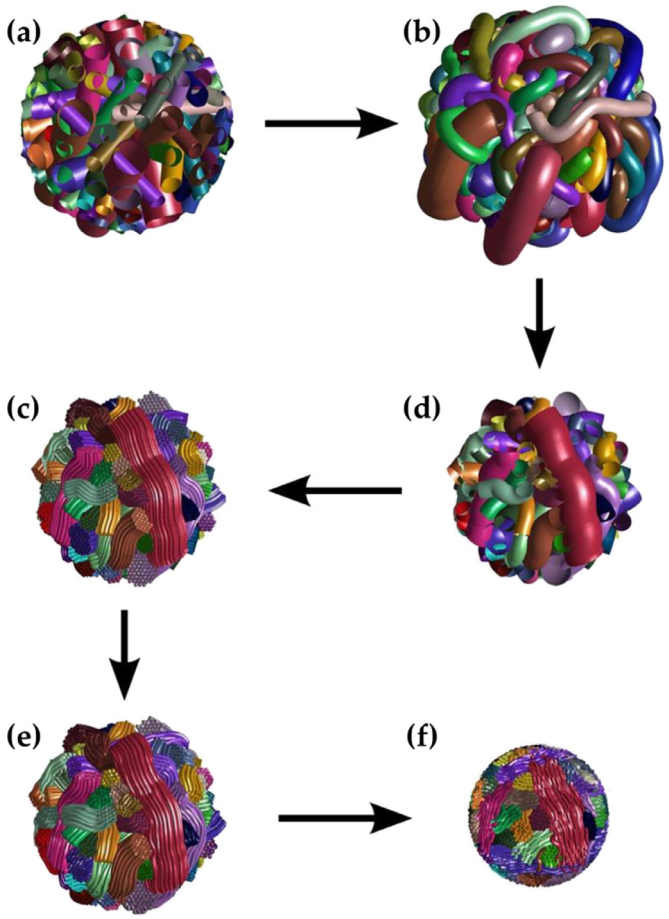

Fig. 15. Illustration of the phantom generation process proposed by Close et al. (2009): (a) initialization with straight tubes, (b) first optimization step to minimize overlap, (c) trimming of bundles to the sphere, (d) generation of sub-bundles, (e) optimization of sub-bundles to minimize overlap and to introduce sub-bundle heterogeneity and (f) trimming of sub-bundles to the final sphere. Figure adapted from Close et al. (2009).

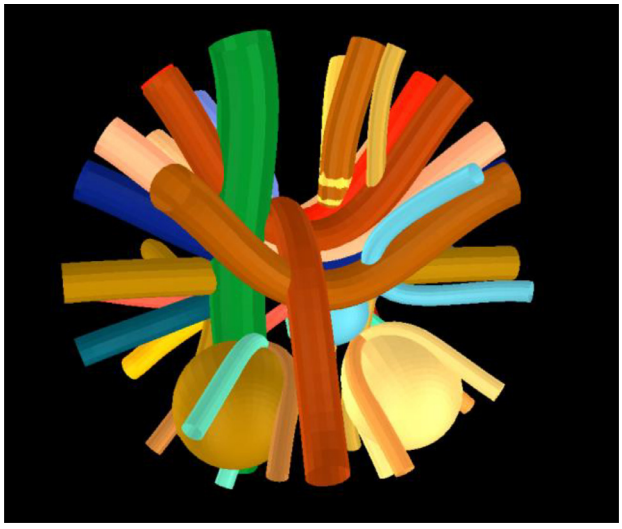

Fig. 16. Illustration of the Phantomas phantom used for 2nd HARDI Reconstruction Challenge[5], organized at ISBI 2013. It consists of 27 fiber bundles, on a 70 × 70 × 70 grid, with 3 spherical CSF regions abstractly mimicking a human brain. Figure created using the Phantomas web interface available on http://www.emmanuelcaruyer.com/phantomas.php.

ical connectome phantoms and code for its generation is available on GitHub.[11]

To quantify the accuracy of tractography estimated connectomes, Tractometer evaluation suite (Côté et al., 2013) proposed two evaluation metrics, namely, number of valid (true positive) and invalid (false positive) bundles. These two metrics were used to evaluate the performance of tractography algorithms for the physical and digital Fibercup phantom (Côté et al., 2013; Neher et al., 2015) and a digital phantom of 25 manually segmented human white matter bundles (Maier-Hein et al., 2017a, 2017b) .

3.5.4. *Advanced MR acquisition simulations for artifact assessment*

Images acquired with dMRI are susceptible to a number of artifacts (Bihan et al., 2006). For example, susceptibility differences at the air-tissue boundary lead to alterations of the B0 field that can cause spatial displacements of several pixels. Subject motion can lead to rigid offsets between images, and eddy currents (EC) lead to distortions of the image in the phase encoding (PE) direction that vary according to the amount of diffusion sensitisation used (typically summarised by the *b*-value) and the direction it is applied in. These artifacts adversely affect analysis of the DW data itself (Irfanoglu et al., 2012), and prevent comparison between the DW images and others that do not contain them, such as T1- and T2-weighted images. They can further lead to spatial offsets between the dMR images in a dataset, further undermining the estimates of microstructure obtained from them.

To assess artifacts in tractography and support development and validation of dMRI artifact removal techniques it is necessary to have numerical simulations. These need to be able to simultaneously model diffusion-weighting contrast and MR physics realistic enough to model artifacts. The simplest numerical methods simply assign a single value of diffusion-weighting contrast to each of the three tissue types, then combine these signals using probabilistic segmentations to form an image (Bastin, 2001, 1999). Other methods use steady-state solutions of the Bloch Equations for the well known pulse sequences to simulate Gibbs ringing (Perrone et al., 2015) noise, partial volume effects, limited spatial and angular resolution in the images (Perrone et al., 2016). However, these methods do not solve directly Bloch Equations to simulate the process of MR acquisition and hence fail to represent the diffusion signal sufficient enough to simulate some of the more complex artifacts such as motion, eddy currents of B0 susceptibility, which Diffusion MRI images are very prone to. Some of the simulators presented in the previous section can simulate a range of complex artifacts (e.g. Fiberfox) however they have mainly focused so far on fiber tractography and tractography validation. There have not been many simulators specifically designed for assessing artifacts.

DW-POSSUM simulator is one such simulator which, because it solves Bloch equations directly, can simulate a range of very complex artifacts (Drobnjak et al., 2006; Graham et al., 2016). It creates realistic diffusion weighting maps from very high resolution HCP (Human Connectome Project) images and combines these with Bloch equation based simulation of MRI images. Bloch equations are solved over a grid with spatially varying values of MR parameters representing the object being imaged, allowing for the most realistic simulations capable of reproduction of a range of image artefacts including eddy currents, susceptibility, Gibbs ringing, ghosting, and chemical shift. An overview of the simulation framework is shown in Fig. 19. POSSUM also simulates arbitrary movement of the object throughout the acquisition of an image and can calculate susceptibility-fields from the input object, taking into account the changing of the susceptibility-induced field with object movement, as well as being able to account for time-varying off-resonance fields, such as those caused by the patient breathing (Drobnjak et al., 2010a, 2010b). POSSUM and DW-POSSUM are included in FSL (FMRIB Software Library) and are openly available as source code and binary ap-

[11] https://github.com/sarwart/deterministic-vs-probabilistic.

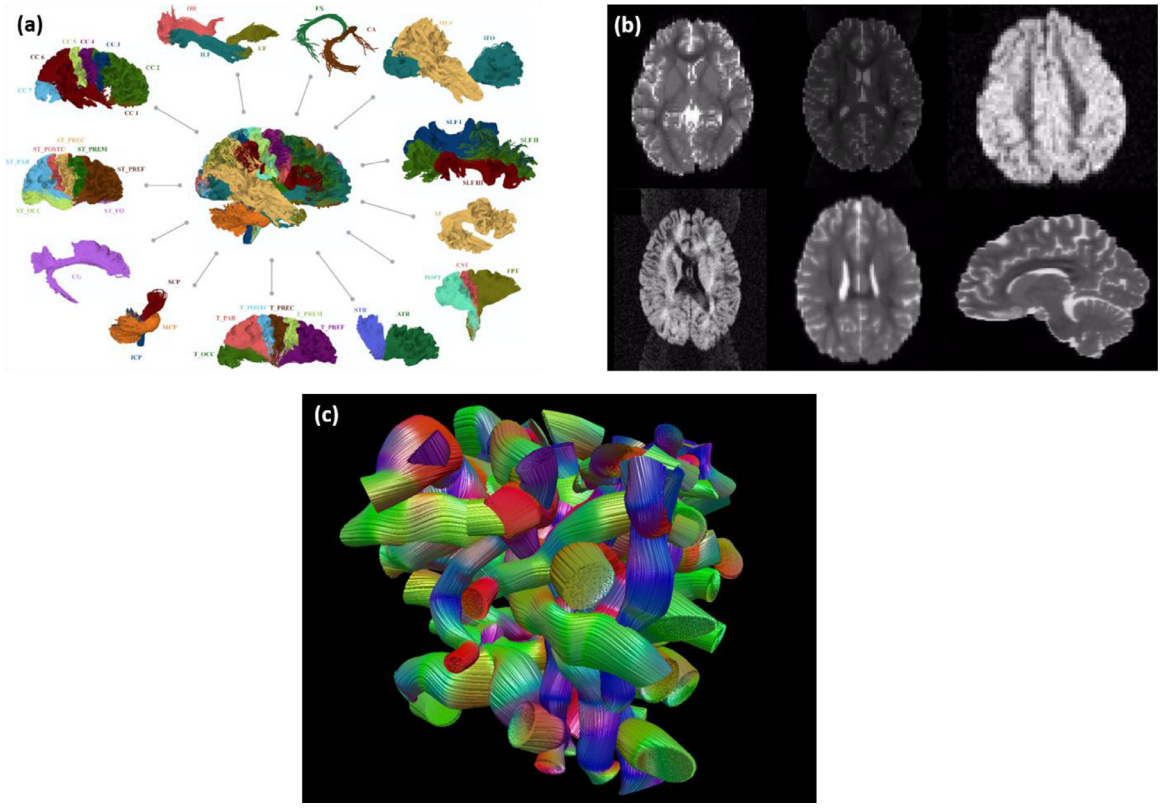

Fig. 17. Illustration the 71 tracts used for the 99 brains Fiberfox simulation (a), exemplary axial slices of one simulated subject of the 99 brains dataset with various artifacts (b), and an exemplary phantom with randomized bundle configuration generated using Fiberfox (c). Figure (a) adapted from Wasserthal et al. (2018).

plication.[12] The complete simulation is controllable via a graphical user interface as well as batch-processing-friendly command line application. Multiple datasets generated with DW-POSSUM are openly available.[13]

Due to its realistic modeling of complex artifacts outlined above DW-POSSUM has been used for a range of applications in assessing artifacts and has contributed directly to development and validation of artifact correction algorithms. Graham et al. showed that one of the most commonly used correction techniques, eddy_correct[10], introduces a systematic error that is significant enough to undermine any analysis performed on data corrected using this scheme (Graham et al., 2016). Andersson et al. (2017) then used it to demonstrate that eddy framework provides a much better alternative, and gave an idea of the level of correction that it can be expected to achieve for commonly acquired datasets. DW-POSSUM was subsequently used also to evaluate eddy's ability to correct for slice outlier artefacts (Andersson et al., 2016).

Susceptibility-by-movement artefact is a phenomenon that is notoriously difficult to study in real data. The susceptibility artefact is caused by an off-resonance field induced by differences in magnetic susceptibility at the air-tissue interface, which cause geometric distortions when data is acquired with an EPI sequence. If the subject moves in the scanner, then the susceptibility field and, in turn, the distortions alter. Whilst the static case is well characterised and studied in the literature (Bihan et al., 2006), comparatively little work has been done to assess the impact of this dynamic case, when the subject moves, and as a result the artefact is rarely considered when acquiring and processing data.

POSSUM's ability to model the interaction between the movement and susceptibility artefact made it a natural test bed to assess the impact of the susceptibility-by-movement artefact. POSSUM can use an air-tissue segmentation to obtain a first-order solution to Maxwell's equations, providing a set of basis functions that describe how the susceptibility field changes with subject movement. This in turn assisted the development of new methods to correct the artefact: (Andersson et al., 2018) proposed a technique to correct for the artefact, and was able to use data simulated with DW-POSSUM (Graham et al. Plos One 2017), alongside real data, to carefully validate the effectiveness of the tool. Further application of the motion model of DW-POSSUM led to correction of slice-to-volume motion (Andersson et al., 2017).

4. Summary and future directions

Phantoms are a necessary tool for creation, optimization and validation of every Diffusion MR imaging pipeline, in particular tractography. They are so essential that, to a certain degree, all tractography research has been using some form of phantom, from in-house builds to more well known publicly accessible ones. So what is an ideal Diffusion MR tractography phantom of the future? Although the answer here depends ultimately on the study in question, one would argue that ultimately each scientist on the diffusion MR imaging pipeline wants a simulation system that can produce realistic anatomical simulated MR images for a variety of different scanning conditions and is fully controllable, accurate, robust, simple to use, fast and easily accessible to all. The development of such a phantom is a very complex task, and both numerical and physical phantoms have their separate complexities.

4.1. Physical phantoms

Physical phantoms are a useful resource for studying the advantages and limitations of both local models of the diffusion process and various fiber tracking algorithms. However, their level of realism with respect to the biological reality of brain white matter remains limited, especially for phantoms made from solid synthetic fibres. Hollow fibres, obtained

[12] http://www.fmrib.ox.ac.uk/fsl/.
[13] https://fsl.fmrib.ox.ac.uk/fsl/fslwiki/POSSUM.

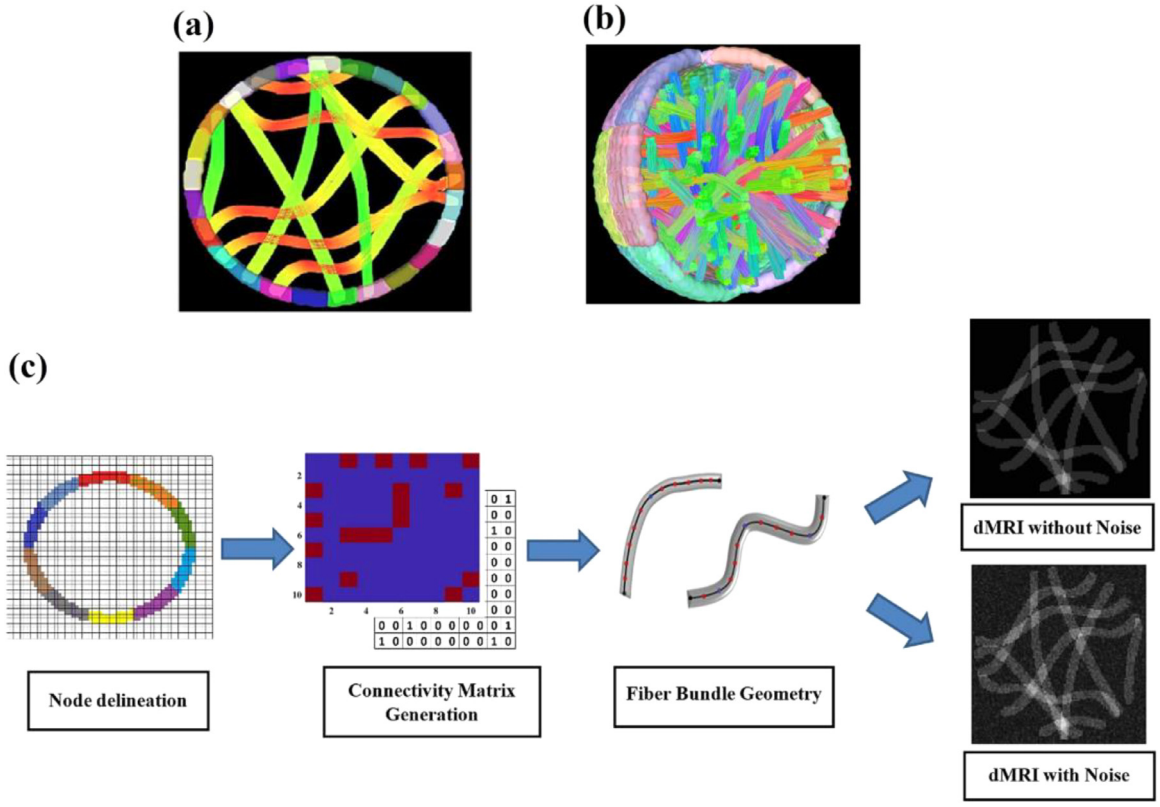

Fig. 18. (a) 2D and (b) 3D dMRI phantoms with predefined connectivity. (c) Schematic of a 2D phantom generation for a 10-node connectome, where nodes are defined on the circumference of a circle (colored segments). The connectivity matrix is predefined for phantoms using generative models, where the connections are realised by simulating tubular fiber bundles. Hence, the simulated dMRI has predefined connectivity which can be used for validating the performance of connectome estimated by tractography algorithm. Figures adapted from Sarwar et al. (2019).

by melt-spinning or electro-spinning techniques, allow a substantial advance in realism by endowing the fibres with an intra-axial compartment and by allowing local deformations that allow deviation from a pure cylindrical shape. Some microstructural details are still missing, such as the control of the thickness of the fiber membrane to allow the creation of a myelin sheath that interrupts at regular intervals to give rise to synthetic Ranvier's nodes. Membranes made of polyethylene or polyester are impermeable which prevents any transfer between the intra-axial and extra-axial compartments and work will have to be carried out on the choice of polymers to be used to control their permeability. Moreover, the cerebral white matter is also populated by glial cells and microdisks which are not modelled today and which will have to be taken into account in the future.

Manufacturing of physical phantoms for diffusion MRI still remains a handmade production and would deserve industrial developments to automate this process in order to be able to create reproducible phantoms with a high degree of realism. Such realistic phantoms would probably stem from back and forth designs between digital phantoms and hardware phantoms to create the ultimate tool for the benchmarking of tractography methods.

Despite innovations in the processes used to construct such as electro-spinning or melt-spinning extrusion techniques, it is unlikely that the level of realism will reach that of real brain white matter tissues. Physical phantoms will mostly remain quality control objects used in the frame of multicenter studies. The dramatic increase in supercomputer computing power and the recent introduction of simulators to create geometric white matter models with a much higher degree of realism than phantoms will undoubtedly further promote the use of digital phantoms in the coming decade.

4.2. Digital phantoms

Digital dMRI phantoms for fiber tractography validation and artifact correction as well as the tools to create them have come a long way over the last decades. They evolved from simply shaped 2D tensor maps to simulations of the actual MR acquisition of a whole brain including complex tissue configurations and realistic MRI effects and artifacts. While conclusions drawn from simulation-based analyses always have to be interpreted extremely carefully and while the state of the art in generating these phantoms is still far from the perfect phantom described in the beginning of this chapter, this discipline has reached a rather mature stage.

Multiple impressive tools to create simulated dMRI phantoms are openly available to and actively used by the tractography community, for example Phantomas,[14] Fiberfox in MITK Diffusion[15] or POSSUM as part of FSL,[16] where Phantomas and Fiberfox are particularly suitable for tractography studies and POSSUM for artifact correction. A number of phantom datasets in this area has been published and used in larger tractography evaluation studies or it is possible to use them in such a way, for example the recently published 99 simulated brains dataset (Neher and Maier-Hein, 2020a, 2020b, 2021), the other Fiberfox simulations (Maier-Hein et al., 2017a, 2017b, 2015; Neher et al., 2017b; Neher and Maier-Hein, 2019), the DW-POSSUM data sets[11] or the Phantomas examples.[17]

[14] http://www.emmanuelcaruyer.com/phantomas.php.
[15] https://github.com/MIC-DKFZ/MITK-Diffusion/.
[16] https://fsl.fmrib.ox.ac.uk/fsl/fslwiki/POSSUM.
[17] https://github.com/ecaruyer/phantomas/tree/master/examples.

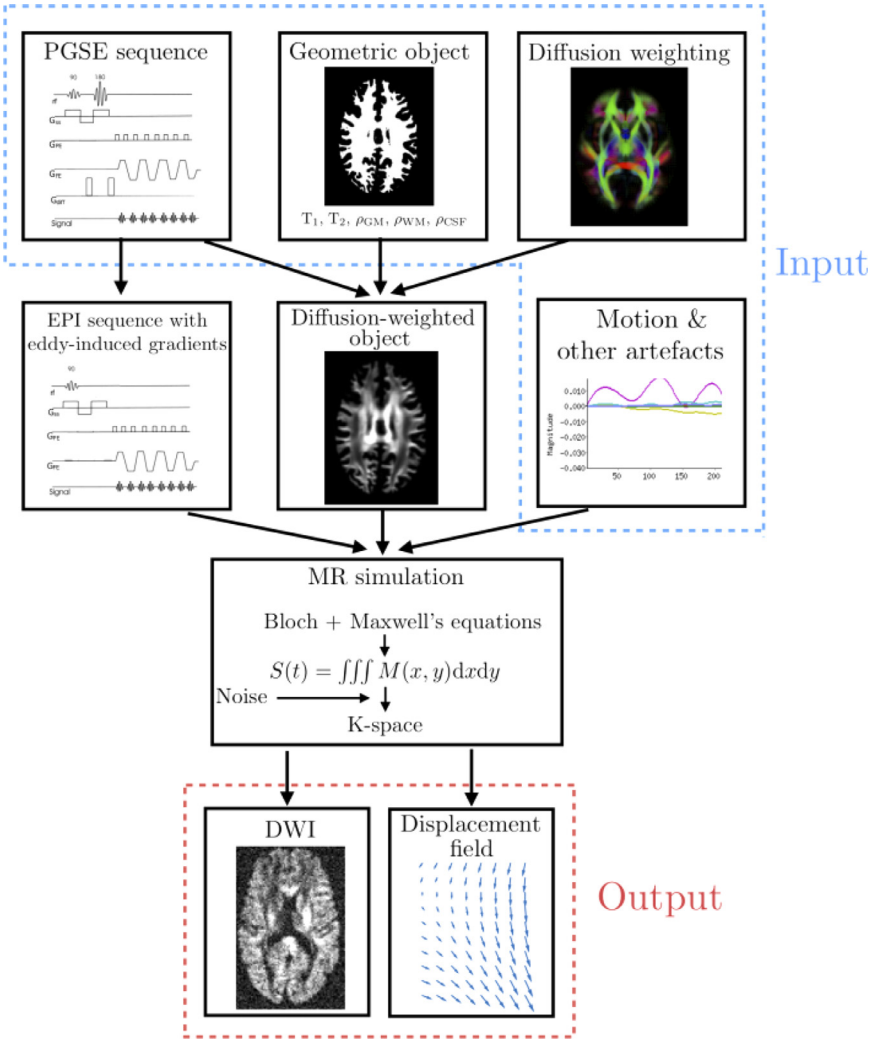

Fig. 19. A conceptual overview of DW-POSSUM. The framework takes four main inputs: a geometric object that specifies the proton density and location of WM, GM and CSF along with their T1 and T2 values; a representation of diffusion-weighting; and a PGSE sequence, detailing RF pulses and gradients. Adapted from Graham et al. (2016).

In the future, some aspects will be particularly important for the field of fiber tractography validation and artifact correction using simulated dMRI data:

Realism: There is still room for improvements in the area of simulations in terms of realism. One particular challenge will be to unify three aspects of a realistic numerical simulation: the cellular microstructure and the corresponding diffusion processes, a tissue macrostructure representative for the human brain; and a comprehensive approximation of a real MR acquisition. There is research already in this direction trying to combine tractography and microstructure together (Daducci et al., 2015a, 2015b) and future work will consist in developing novel types of ultra-realistic numerical phantoms. Such phantoms should rely on the simulation of highly realistic geometries taking into account all cell types populating white matter: myelinated and unmyelinated axonal fibers, glial cells including microglia, oligodendrocytes and astrocytes, microvasculature, and even neurons. Furthermore, a range of different pathologies need to be included in simulations, and these have only just been started to be explored, e.g. tumor growth models in Jackson et al. (2020) and epilepsy models in (Nielsen et al., 2021). Another aspect is that the synthesis of the diffusion signal attenuation should be based on least-assumption approaches to avoid modeling bias. Monte-Carlo simulations are not assumption-free, but they are the least assumption-intensive and can be most easily modified to better fit the biophysical reality. Finally, simulations need to be up-to-date with the new developments in the field of MR imaging. MR imaging is evolving rapidly and we are seeing much more powerful hardware systems with extremely strong magnetic fields, strong gradient coils, much higher resolutions, etc. These developments are pushing the boundaries of the MR imaging field in identifying new contrasts, however, they also bring with them a range of new challenges such as more prominent effects or presence of totally new artefacts. Future simulation systems and phantoms need to be flexible and continually develop in order to keep up with these new developments.

Computational prowess: With the evolving degrees of complexity and realism of simulation systems there is a strong need for powerful computational hardware and simulation speed. Incorporating all of the realistic scanner and object effects creates a huge demand on the computational memory and time. The input object itself that describes the MR properties of the simulated brain/body can take thousands of GB of memory. To run a single MRI simulation of full Bloch equations with all of the features described can take hours. These problems are possibly the most pressing and have so far prevented many of the simulators from simulating fully realistic DIffusion MR images. New developments in GPU programming, and increasing power of computers will be crucial here in driving future research and developing new ways of parallelising and speeding up the simulation process.

Available data: There is still a lack of large and variable openly available simulated datasets, including various image contrasts, anatomies, pathologies as well as variable MR acquisition settings. Such large and variable datasets become increasingly important with the rise of machine learning and AI in the area of dMRI research. In this context, reaching a consensus in the community on how to evaluate, with what

tools, on which data and with which metrics (Maier-Hein et al., 2018; Reinke et al., 2018) is a non-trivial task and will gain increasing importance.

4.3. Assessing artifacts, quality control and AI

One of the very important aspects of artifact assessment in Diffusion MRI is quality control (QC). QC involves ensuring a dataset meets a certain set of standards before the dataset is given the clearance for inclusion in subsequent analyses. Diffusion MRI has unique challenges that make manual QC particularly difficult, including a greater number of artefacts than other MR modalities and a greater volume of data. The gold standard is manual inspection of the data, but this process is time-consuming and subjective. The current trend towards acquiring increasingly large datasets means the time required for human QC is becoming prohibitive. The HCP (Van Essen et al., 2012) acquired data for 1200 subjects with almost 300 dMR volumes per subject and the UK Biobank will eventually acquire imaging data for 100,000 subjects with over 100 vol per subject (Miller et al., 2016).

Recently supervised learning approaches based on convolutional neural networks (CNNs) have been shown to be competitive with manual inspection. However, CNNs tend to have many parameters requiring optimization — often in the millions — meaning they typically require large, manually labelled datasets for training which can be very challenging as is itself time-consuming to produce and still introduces an element of subjectivity. One potential way to address these issues is to use simulated data. Simulation could circumvent the need for human labeling by producing realistic datasets, along with ground-truth labels, for training machine learning tools on. In the case of QC, a simulator that was capable of producing datasets containing artefacts, such as motion, could be used to produce a training set. Little research has been done to investigate the feasibility of a simulation-based approach to training supervised learning tools. DW-POSSUM was first to demonstrate that the need for manual labeling can be greatly reduced by training on simulated data, and using a small amount of labelled data for a final calibration step (Graham et al., 2018). They demonstrate its potential for the detection of severe movement artefacts, and compare performance to a classifier trained on manually-labelled real data.

Work such as this suggests that hybrid approaches, combining large amounts of simulated data with smaller amounts of real, labelled data, offer the opportunity to develop performance machine learning tools whilst drastically reducing the need for labelled data. Similar examples are also being developed outside of Diffusion MRI: (Borges et al., 2019) simulate MR scans with varying sequence parameters in order to develop segmentation tools that are invariant to MR-physics; (Billot et al., 2020) simulate data containing extreme contrast variations was used to train modality-agnostic segmentation tools; (Shaw et al., 2020), the authors show that simulated data with movement artefacts can be used to train networks to remove movement artefacts from data. These suggest a trend in which with the rise of larger and larger data sets and development and use of machine learning techniques that go with it, the need for numerical simulations will become even greater.

4.4. Outlook

The impact of the human connectome project on science, healthcare and society in general is highly dependent on validity, robustness and quality of the data which can only truly be measured with ground truth obtained from the phantoms. It is hence extremely important to address the challenges mentioned above and create phantoms that can be used reliably for validation of tractography and assessment of artifacts. Additionally, we as a research community should also work harder to establish stronger collaborations between the scientists that work on data processing methods and those that work on validation and phantoms. This would align the speed of the two and improve the work of both, phantoms would inform methods development and validation and phantom development would be more guided and focused on the needs that can create the most impact. In the future that is becoming more and more digital, data sets ever so larger and AI, with its need for highly controllable large ground truth training data sets, becoming a norm, the need and importance of physical and numerical phantoms and simulations will only grow.

Credit author statement

Ivana Drobnjak: Advanced MR acquisitions and Artifact Assessment**;** Summary and Future Directions**; Peter Neher:** Digital Phantoms**; Tabinda Sarwar:** Introduction, Simulating Connectomic Networks; **Cyril Poupon:** Physical Phantoms

Acknowledgment

This work was supported by the German Research Foundation (DFG) grant numbers MA6340/10-1 and MA6340/12-1.

References

Abu-Sardanah, S.O., Hussain, U., Moore, J., Baron, C., Peters, T., Khan, A.R., 2018. Design and evaluation of a diffusion MRI fibre phantom using 3D printing. In: Proceedings of the Medical Imaging 2018: Physics of Medical Imaging. International Society for Optics and Photonics doi:10.1117/12.2293566.

Aganj, I., Lenglet, C., Jahanshad, N., Yacoub, E., Harel, N., Thompson, P.M., Sapiro, G., 2011. A Hough transform global probabilistic approach to multiple-subject diffusion MRI tractography. Med. Image Anal. 15, 414–425.

Alexander, D.C., Dyrby, T.B., Nilsson, M., Zhang, H., 2019. Imaging brain microstructure with diffusion MRI: practicality and applications. NMR Biomed. 32, e3841. doi:10.1002/nbm.3841.

Andersson, J.L.R., Graham, M.S., Drobnjak, I., Zhang, H., Campbell, J., 2018. Susceptibility-induced distortion that varies due to motion: correction in diffusion MR without acquiring additional data. Neuroimage 171, 277–295. doi:10.1016/j.neuroimage.2017.12.040.

Andersson, J.L.R., Graham, M.S., Drobnjak, I., Zhang, H., Filippini, N., Bastiani, M., 2017. Towards a comprehensive framework for movement and distortion correction of diffusion MR images: within volume movement. Neuroimage 152, 450–466. doi:10.1016/j.neuroimage.2017.02.085.

Andersson, J.L.R., Graham, M.S., Zsoldos, E., Sotiropoulos, S.N., 2016. Incorporating outlier detection and replacement into a non-parametric framework for movement and distortion correction of diffusion MR images. Neuroimage 141, 556–572. doi:10.1016/j.neuroimage.2016.06.058.

Assaf, Y., Basser, P.J., 2005. Composite hindered and restricted model of diffusion (CHARMED) MR imaging of the human brain. Neuroimage 27, 48–58.

Bach, M., Fritzsche, K.H., Stieltjes, B., Laun, F.B., 2013. Investigation of resolution effects using a specialized diffusion tensor phantom. Magn. Reson. Med..

Barbieri, S., Klein, J., Nimsky, C., Hahn, H.K., 2010. Assessing fiber tracking accuracy via diffusion tensor software models. In: Proceedings of the SPIE 7623, Medical Imaging 2010: Image Processing.

Basser, P.J., Mattiello, J., Ihan, D.L.B., 1994. Estimation of the effective self-diffusion tensor from the NMR spin echo. J. Magn. Reson. B 103, 247–254.

Bastin, M.E., 1999. Correction of eddy current-induced artefacts in diffusion tensor imaging using iterative cross-correlation. Magn. Reson. Imaging 17, 1011–1024. doi:10.1016/S0730-725X(99)00026-0.

Bastin, M.E., 2001. On the use of the FLAIR technique to improve the correction of eddy current induced artefacts in MR diffusion tensor imaging. Magn. Reson. Imaging 19, 937–950. doi:10.1016/S0730-725X(01)00427-1.

Batchelor, P.G., Calamante, F., Tournier, J.D., Atkinson, D., Hill, D.L.G., Connelly, A., 2006. Quantification of the shape of fiber tracts. Magn. Reson. Med. 55, 894–903.

Benou, I., Riklin Raviv, T., et al., 2019. DeepTract: a probabilistic deep learning framework for white matter fiber tractography. In: Shen, D., Liu, T., Peters, T.M., Staib, L.H., Essert, C., Zhou, S., et al. (Eds.), Medical Image Computing and Computer Assisted Intervention – MICCAI 2019, Lecture Notes in Computer Science. Springer International Publishing, Cham, pp. 626–635. doi:10.1007/978-3-030-32248-9_70.

Betzel, R.F., Avena-Koenigsberger, A., Goñi, J., He, Y., de Reus, M.A., Griffa, A., Vértes, P.E., Mišic, B., Thiran, J.P., Hagmann, P., van den Heuvel, M., Zuo, X.N., Bullmore, E.T., Sporns, O., 2016. Generative models of the human connectome. Neuroimage 124, 1054–1064. doi:10.1016/j.neuroimage.2015.09.041.

Bihan, D.L., Poupon, C., Amadon, A., Lethimonnier, F., 2006. Artifacts and pitfalls in diffusion MRI. J. Magn. Reson. Imaging 24, 478–488. doi:10.1002/jmri.20683.

Billot, B., Greve, D.N., Leemput, K.V., Fischl, B., Iglesias, J.E., Dalca, A., 2020. A learning strategy for contrast-agnostic MRI segmentation. In: Medical Imaging with Deep Learning. PMLR, pp. 75–93 Presented at proceedings of the medical imaging with deep learning.

Borges, P., Sudre, C., Varsavsky, T., Thomas, D., Drobnjak, I., Ourselin, S., Cardoso, M.J., 2019. Physics-informed brain MRI segmentation. Lecture Notes in Computer Science [WWW Document] Subser. Lect. Notes Artif. Intell. Lect. Notes BioinformaURL(accessed 4.6.21) doi:10.1007/978-3-030-32778-1_11.

Bressler, S.L., Menon, V., 2010. Large-scale brain networks in cognition: emerging methods and principles. Trends Cogn. Sci. 14, 277–290. doi:10.1016/j.tics.2010.04.004.

Burcaw, L.M., Fieremans, E., Novikov, D.S., 2015. Mesoscopic structure of neuronal tracts from time-dependent diffusion. Neuroimage 114, 18–37. doi:10.1016/j.neuroimage.2007.04.067.

Calabrese, E., Badea, A., Cofer, G., Qi, Y., Johnson, G.A., 2015. A diffusion MRI tractography connectome of the mouse brain and comparison with neuronal tracer data. Cereb. Cortex 25, 4628–4637. doi:10.1093/cercor/bhv121, N. Y. N 1991.

Campbell, J.S.W., Savadjiev, P., Siddiqi, K., Pike, G.B., 2006. Validation and regularization in diffusion MRI tractography. In: Proceedings of the 3rd IEEE International Symposium on Biomedical Imaging: Nano to Macro, pp. 351–354. doi:10.1109/ISBI.2006.1624925 Presented at the 3rd IEEE International Symposium on Biomedical Imaging: Nano to Macro, 2006.

Caruyer, E., Daducci, A., Descoteaux, M., Houde, J.C., Thiran, J.P., Verma, R., 2014. Phantomas: a flexible software library to simulate diffusion MR phantoms. In: Proceedings of the ISMRM.

Casey, B.J., Tottenham, N., Liston, C., Durston, S., 2005. Imaging the developing brain: what have we learned about cognitive development? Trends Cogn. Sci. 9, 104–110. doi:10.1016/j.tics.2005.01.011.

Cetingul, H.E., \cC, H.E., etingü, l, Nadar, M., Thompson, P., Sapiro, G., Lenglet, C., 2012. Simultaneous ODF estimation and tractography in HARDI. In: Proceedings of the Engineering in Medicine and Biology Society (EMBC), Annual International Conference of the IEEE, pp. 86–89.

Chen, B., Song, A.W., 2008. Diffusion tensor imaging fiber tracking with local tissue property sensitivity: phantom and in vivo validation. Magn. Reson. Imaging 26, 103–108.

Ciccarelli, O., Catani, M., Johansen-Berg, H., Clark, C., Thompson, A., 2008. Diffusion-based tractography in neurological disorders: concepts, applications, and future developments. Lancet Neurol. 7, 715–727. doi:10.1016/S1474-4422(08)70163-7.

Close, T.G., Tournier, J.D., Calamante, F., Johnston, L.A., Mareels, I., Connelly, A., 2009. A software tool to generate simulated white matter structures for the assessment of fibre-tracking algorithms. Neuroimage 47, 1288–1300.

Côté, M.A., Girard, G., Bore, A., Garyfallidis, E., Houde, J.C., Descoteaux, M., 2013. Tractometer: towards validation of tractography pipelines. Med. Image Anal. 17. doi:10.1016/j.media.2013.03.009.

Daducci, A., Dal Palú, A., Descoteaux, M., Thiran, J.P., 2016. Microstructure informed tractography: pitfalls and open challenges. Front. Neurosci. 10.

Daducci, A., Palù, A.D., Lemkaddem, A., Thiran, J., 2015a. COMMIT: convex optimization modeling for microstructure informed tractography. IEEE Trans. Med. Imaging 34, 246–257. doi:10.1109/TMI.2014.2352414.

Daducci, Alessandro, Dal Palù, A., Lemkaddem, A., Thiran, J.P., 2015b. COMMIT: convex optimization modeling for microstructure informed tractography. IEEE Trans. Med. Imaging 34, 246–257.

D'Arceuil, H.E., Westmoreland, S., de Crespigny, A.J., 2007. An approach to high resolution diffusion tensor imaging in fixed primate brain. Neuroimage 35, 553–565. doi:10.1016/j.neuroimage.2006.12.028.

Dauguet, J., Peled, S., Berezovskii, V., Delzescaux, T., Warfield, S.K., Born, R., Westin, C.F., 2007. Comparison of fiber tracts derived from *in-vivo* DTI tractography with 3D histological neural tract tracer reconstruction on a macaque brain. Neuroimage 37, 530–538. doi:10.1016/j.neuroimage.2007.04.067.

Delputte, S., Fieremans, E., De Deene, Y., D'Asseler, Y., Achten, E., Lemahieu, I., Van de Walle, R., 2006. Quantitative validation of white matter fiber tractography by use of an anatomically realistic synthetic diffusion tensor phantom. In: Proceedings of the ISMRM 14th Scientific Meeting & Exhibition.

Drobnjak, I., Gavaghan, D., Süli, E., Pitt-Francis, J., Jenkinson, M., 2006. Development of a functional magnetic resonance imaging simulator for modeling realistic rigid-body motion artifacts. Magn. Reson. Med. 56, 364–380. doi:10.1002/mrm.20939.

Drobnjak, I., Pell, G.S., Jenkinson, M., 2010a. Simulating the effects of time-varying magnetic fields with a realistic simulated scanner. Magn. Reson. Imaging 28, 1014–1021. doi:10.1016/j.mri.2010.03.029.

Drobnjak, I., Siow, B., Alexander, D.C., 2010b. Optimizing gradient waveforms for microstructure sensitivity in diffusion-weighted MR. J. Magn. Reson. 206, 41–51. doi:10.1016/j.jmr.2010.05.017.

Drobnjak, I., Zhang, H., Hall, M.G., Alexander, D.C., 2011. The matrix formalism for generalised gradients with time-varying orientation in diffusion NMR. J. Magn. Reson. 210, 151–157. doi:10.1016/j.jmr.2011.02.022.

Dyrby, T.B., Søgaard, L.V., Parker, G.J., Alexander, D.C., Lind, N.M., Baaré, W.F.C., Hay-Schmidt, A., Eriksen, N., Pakkenberg, B., Paulson, O.B., Jelsing, J., 2007. Validation of in vitro probabilistic tractography. Neuroimage 37, 1267–1277. doi:10.1016/j.neuroimage.2007.06.022.

Fan, Q., Nummenmaa, A., Wichtmann, B., Witzel, T., Mekkaoui, C., Schneider, W., Huang, S.Y., 2018a. Validation of diffusion MRI estimates of compartment size and volume fraction in a biomimetic brain phantom using a human MRI scanner with 300 mT/m maximum gradient strength. Neuroimage 182, 469–478.

Fan, Q., Nummenmaa, A., Wichtmann, B., Witzel, T., Mekkaoui, C., Schneider, W., Wald, L.L., Huang, S.Y., 2018b. Validation of diffusion MRI estimates of compartment size and volume fraction in a biomimetic brain phantom using a human MRI scanner with 300 mT/m maximum gradient strength. NeuroImage Microstruct. Imaging 182, 469–478. doi:10.1016/j.neuroimage.2018.01.004.

Farrher, E., Kaffanke, J., Celik, A.A., Stöcker, T., Grinberg, F., Shah, N.J., 2012. Novel multisection design of anisotropic diffusion phantoms. Magn. Reson. Imaging 30 (4), 518–526.

Farrher, E., Lindemeyer, J., Grinberg, F., Oros-Peusquens, A.M., Shah, N.J., 2017. Concerning the matching of magnetic susceptibility differences for the compensation of background gradients in anisotropic diffusion fibre phantoms. PLoS ONE 12, e0176192. doi:10.1371/journal.pone.0176192.

Fieremans, E., De Deene, Y., Delputte, S., Özdemir, M.S., D'Asseler, Y., Vlassenbroeck, J., Deblaere, K., Achten, E., Lemahieu, I., 2008. Simulation and experimental verification of the diffusion in an anisotropic fiber phantom. J. Magn. Reson. 190, 189–199. doi:10.1016/j.jmr.2007.10.014.

Fieremans, E., Deene, Y.D., 2020. Chapter 11:gel phantoms for diffusion MRI studies. In: NMR and MRI of Gels, pp. 379–400. doi:10.1039/9781788013178-00379.

Fieremans, E., Lee, H.H., 2018. Physical and numerical phantoms for the validation of brain microstructural MRI: a cookbook. Neuroimage 182, 39–61. doi:10.1016/j.neuroimage.2018.06.046.

Fillard, P., Descoteaux, M., Goh, A., Gouttard, S., Jeurissen, B., Malcolm, J., Ramirez-Manzanares, A., Reisert, M., Sakaie, K., Tensaouti, F., Yo, T., Mangin, J.F., Poupon, C., 2011. Quantitative evaluation of 10 tractography algorithms on a realistic diffusion MR phantom. Neuroimage 56, 220–234. doi:10.1016/j.neuroimage.2011.01.032.

Ginsburger, K., Matuschke, F., Poupon, F., Mangin, J.F., Axer, M., Poupon, C., 2019. MEDUSA: a GPU-based tool to create realistic phantoms of the brain microstructure using tiny spheres. Neuroimage 193, 10–24. doi:10.1016/j.neuroimage.2019.02.055.

Ginsburger, K., Poupon, F., Beaujoin, J., Estournet, D., Matuschke, F., Mangin, J.F., Axer, M., Poupon, C., 2018. Improving the realism of white matter numerical phantoms: a step toward a better understanding of the influence of structural disorders in diffusion MRI. Front. Phys. 6. doi:10.3389/fphy.2018.00012.

Girard, G., Caminiti, R., Battaglia-Mayer, A., St-Onge, E., Ambrosen, K.S., Eskildsen, S.F., Krug, K., Dyrby, T.B., Descoteaux, M., Thiran, J.P., Innocenti, G.M., 2020. On the cortical connectivity in the macaque brain: a comparison of diffusion tractography and histological tracing data. Neuroimage 221, 117201. doi:10.1016/j.neuroimage.2020.117201.

Gössl, C., Fahrmeir, L., Pütz, B., Auer, L.M., Auer, D.P., 2002. Fiber tracking from DTI using linear state space models: detectability of the pyramidal tract. Neuroimage 16, 378–388.

Graham, M.S., Drobnjak, I., Zhang, H., 2016. Realistic simulation of artefacts in diffusion MRI for validating post-processing correction techniques. Neuroimage 125, 1079–1094. doi:10.1016/j.neuroimage.2015.11.006.

Graham, M.S., Drobnjak, I., Zhang, H., 2018. A supervised learning approach for diffusion MRI quality control with minimal training data. Neuroimage 178, 668–676. doi:10.1016/j.neuroimage.2018.05.077.

Grebenkov, D.S., 2011. A fast random walk algorithm for computing the pulsed-gradient spin-echo signal in multiscale porous media. J. Magn. Reson. 208, 243–255.

Grech-Sollars, M., Zhou, F.L., Waldman, A.D., Parker, G.J.M., Hubbard Cristinacce, P.L., 2018. Stability and reproducibility of co-electrospun brain-mimicking phantoms for quality assurance of diffusion MRI sequences. Neuroimage 181, 395–402. doi:10.1016/j.neuroimage.2018.06.059.

Gudbjartsson, H., Patz, S., 1995. The rician distribution of noisy MRI data. Magn. Reson. Med. 34, 910–914.

Guise, C., Fernandes, M.M., Nóbrega, J.M., Pathak, S., Schneider, W., Fangueiro, R., 2016. Hollow polypropylene yarns as a biomimetic brain phantom for the validation of high-definition fiber tractography imaging. ACS Appl. Mater. Interfaces 8, 29960–29967. doi:10.1021/acsami.6b09809.

Guye, M., Parker, G.J.M., Symms, M., Boulby, P., Wheeler-Kingshott, C.A.M., Salek-Haddadi, A., Barker, G.J., Duncan, J.S., 2003. Combined functional MRI and tractography to demonstrate the connectivity of the human primary motor cortex *in vivo*. Neuroimage 19, 1349–1360. doi:10.1016/s1053-8119(03)00165-4.

Hau, J., Sarubbo, S., Houde, J.C., Corsini, F., Girard, G., Deledalle, C., Crivello, F., Zago, L., Mellet, E., Jobard, G., Joliot, M., Mazoyer, B., Tzourio-Mazoyer, N., Descoteaux, M., Petit, L., 2017. Revisiting the human uncinate fasciculus, its subcomponents and asymmetries with stem-based tractography and microdissection validation. Brain Struct. Funct. 222, 1645–1662. doi:10.1007/s00429-016-1298-6.

Hellerbach, A., Schuster, V., Jansen, A., Sommer, J., 2013. MRI phantoms – are there alternatives to agar? PLoS ONE 8, e70343. doi:10.1371/journal.pone.0070343.

Huang, C.C., Hsu, C.-C.H., Zhou, F.L., Kusmia, S., Drakesmith, M., Parker, G.J.M., Lin, C.P., Jones, D.K., 2021. Validating pore size estimates in a complex microfiber environment on a human MRI system. Magn. Reson. Med. 86, 1514–1530. doi:10.1002/mrm.28810.

Hubbard, P.L., Parker, G.J.M., 2009. Chapter 16 - validation of tractography. In: Johansen-Berg, H., Behrens, T.E.J. (Eds.), Diffusion MRI. Academic Press, San Diego, pp. 353–375. doi:10.1016/B978-0-12-374709-9.00016-X.

Hubbard, P.L., Zhou, F.L., Eichhorn, S.J., Parker, G.J.M., 2015. Biomimetic phantom for the validation of diffusion magnetic resonance imaging. Magn. Reson. Med. 73, 299–305. doi:10.1002/mrm.25107.

Ianuş, A., Alexander, D.C., Drobnjak, I., 2016. Microstructure imaging sequence simulation toolbox. In: Tsaftaris, S.A., Gooya, A., Frangi, A.F., Prince, J.L. (Eds.), Simulation and Synthesis in Medical Imaging, Lecture Notes in Computer Science. Springer International Publishing, Cham, pp. 34–44. doi:10.1007/978-3-319-46630-9_4.

Ianuş, A., Siow, B., Drobnjak, I., Zhang, H., Alexander, D.C., 2013. Gaussian phase distribution approximations for oscillating gradient spin echo diffusion MRI. J. Magn. Reson. 227, 25–34. doi:10.1016/j.jmr.2012.11.021.

Irfanoglu, M.O., Walker, L., Sarlls, J., Marenco, S., Pierpaoli, C., 2012. Effects of image distortions originating from susceptibility variations and concomitant fields on diffusion MRI tractography results. Neuroimage 61, 275–288. doi:10.1016/j.neuroimage.2012.02.054.

Jackson, P.R., Hawkins-Daarud, A., Swanson, K.R., 2020. Simulated diffusion weighted images based on model-predicted tumor growth. In: Proceedings of the Simulation and Synthesis in Medical Imaging - 5th International Workshop, SASHIMI 2020, Held in Conjunction with MICCAI 2020, Proceedings. Springer Science and Business Media Deutschland GmbH, pp. 32–40. doi:10.1007/978-3-030-59520-3_4 Presented at the 5th International Workshop on Simulation and Synthesis in Medical Imaging, SASHIMI 2020, held in conjunction with the Medical Image Computing and Computer Assisted Intervention, MICCAI 2020.

Jeurissen, B., Leemans, A., Jones, D.K., Tournier, J.D., Sijbers, J., 2011. Probabilistic fiber

tracking using the residual bootstrap with constrained spherical deconvolution. Hum. Brain Mapp. 32, 461–479.
Jones, D.K., Cercignani, M., 2010. Twenty-five pitfalls in the analysis of diffusion MRI data. NMR Biomed. 23, 803–820. doi:10.1002/nbm.1543.
Kang, N., Zhang, J., Carlson, E.S., Gembris, D., 2005. White matter fiber tractography via anisotropic diffusion simulation in the human brain. IEEE Trans. Med. Imaging 24, 1127–1137.
Keenan, K.E., Ainslie, M., Barker, A.J., Boss, M.A., Cecil, K.M., Charles, C., Zheng, J., 2018a. Quantitative magnetic resonance imaging phantoms: a review and the need for a system phantom. Magn. Reson. Med. 79 (1), 48–61. doi:10.1371/journal.pone.0008595.
Keenan, K.E., Ainslie, M., Barker, A.J., Boss, M.A., Cecil, K.M., Charles, C., Chenevert, T.L., Clarke, L., Evelhoch, J.L., Finn, P., Gembris, D., Gunter, J.L., Hill, D.L.G., Jack, C.R., Jackson, E.F., Liu, G., Russek, S.E., Sharma, S.D., Steckner, M., Stupic, K.F., Trzasko, J.D., Yuan, C., Zheng, J., 2018b. Quantitative magnetic resonance imaging phantoms: a review and the need for a system phantom. Magn. Reson. Med. 79, 48–61. doi:10.1002/mrm.26982.
Khalsa, S., Mayhew, S.D., Chechlacz, M., Bagary, M., Bagshaw, A.P., 2014. The structural and functional connectivity of the posterior cingulate cortex: comparison between deterministic and probabilistic tractography for the investigation of structure-function relationships. Neuroimage 102 (Pt 1), 118–127. doi:10.1016/j.neuroimage.2013.12.022.
Khundrakpam, B.S., Reid, A., Brauer, J., Carbonell, F., Lewis, J., Ameis, S., Karama, S., Lee, J., Chen, Z., Das, S., Evans, A.C.Brain Development Cooperative Group, 2013. Developmental changes in organization of structural brain networks. Cereb. Cortex 23, 2072–2085. doi:10.1093/cercor/bhs187, N. Y. N 1991.
Knösche, T.R., Anwander, A., Liptrot, M., Dyrby, T.B., 2015. Validation of tractography: comparison with manganese tracing. Hum. Brain Mapp. 36, 4116–4134. doi:10.1002/hbm.22902.
Kreher, B.W., Schneider, J.F., Mader, I., Martin, E., Hennig, J., Il'Yasov, K.A., 2005. Multitensor approach for analysis and tracking of complex fiber configurations. Magn. Reson. Med. 54, 1216–1225.
Laun, F.B., 2012. Multiple correlation function tool.
Laun, F.B., Huff, S., Stieltjes, B., 2009. On the effects of dephasing due to local gradients in diffusion tensor imaging experiments: relevance for diffusion tensor imaging fiber phantoms. Magn. Reson. Imaging 27, 541–548.
Lawes, I.N.C., Barrick, T.R., Murugam, V., Spierings, N., Evans, D.R., Song, M., Clark, C.A., 2008. Atlas-based segmentation of white matter tracts of the human brain using diffusion tensor tractography and comparison with classical dissection. Neuroimage 39, 62–79. doi:10.1016/j.neuroimage.2007.06.041.
Lazar, M., Alexander, A.L., 2001. Error analysis of white matter tracking algorithms (streamlines and tensorlines) for DT-MRI. Proc. Int. Soc. Magn. Reson. Med. 506 Glasg. UK.
Lazar, M., Alexander, A.L., 2003. An error analysis of white matter tractography methods: synthetic diffusion tensor field simulations. Neuroimage 20, 1140–1153.
Lee, H.H., Fieremans, E., Novikov, D.S., 2021. Realistic Microstructure Simulator (RMS): monte Carlo simulations of diffusion in three-dimensional cell segmentations of microscopy images. J. Neurosci. Methods 350, 109018. doi:10.1016/j.jneumeth.2020.109018.
Leemans, A., Sijbers, J., Verhoye, M., Van der Linden, A., Van Dyck, D., 2005. Mathematical framework for simulating diffusion tensor MR neural fiber bundles. Magn. Reson. Med. 53, 944–953.
Leergaard, T.B., White, N.S., Crespigny, A.de, Bolstad, I., D'Arceuil, H., Bjaalie, J.G., Dale, A.M., 2010. Quantitative histological validation of diffusion MRI fiber orientation distributions in the rat brain. PLoS ONE 5, e8595. doi:10.1371/journal.pone.0008595.
Lemberskiy, G., Baete, S.H., Cloos, M.A., Novikov, D.S., Fieremans, E., 2017. Validation of surface-to-volume ratio measurements derived from oscillating gradient spin echo on a clinical scanner using anisotropic fiber phantoms. NMR Biomed. 30 (5), e3708. doi:10.1007/978-3-030-00937-3_45.
Lin, C.P., Wedeen, V.J., Chen, J.H., Yao, C., Tseng, W.-Y.I., 2003. Validation of diffusion spectrum magnetic resonance imaging with manganese-enhanced rat optic tracts and ex vivo phantoms. Neuroimage 19, 482–495. doi:10.1016/s1053-8119(03)00154-x.
Lorenz, R., Bellemann, M.E., Hennig, J., Il'yasov, K.A., 2008. Anisotropic phantoms for quantitative diffusion tensor imaging and fiber-tracking validation. Appl. Magn. Reson. 33, 419. doi:10.1007/s00723-008-0087-7.
Lori, N., Akbudak, E., Snyder, A., Shimony, J., Conturo, T., 2000. Diffusion tensor tracking of human neuronal fiber bundles: simulation of effects of noise, voxel size and data interpolation, p. 775.
Lori, N.F., Akbudak, E., Shimony, J.S., Cull, T.S., Snyder, A.Z., Guillory, R.K., Conturo, T.E., 2002. Diffusion tensor fiber tracking of human brain connectivity: aquisition methods, reliability analysis and biological results. NMR Biomed. 15, 494–515.
Maier-Hein, K., Neher, P., Houde, J.C., Caruyer, E., Daducci, A., Dyrby, T., Stieltjes, B., Descoteaux, M., 2015. Tractography challenge ISMRM 2015 data. 10.5281/zenodo.572345
Maier-Hein, K., Neher, P., Houde, J.C., Caruyer, E., Daducci, A., Dyrby, T., Stieltjes, B., Descoteaux, M., 2017. Tractography challenge ISMRM 2015 high-resolution data. 10.5281/zenodo.579933
Maier-Hein, K.H., Neher, P.F., Houde, J.C., Côté, M.A., Garyfallidis, E., Zhong, J., Chamberland, M., Yeh, F.C., Lin, Y.C., Ji, Q., Reddick, W.E., Glass, J.O., Chen, D.Q., Feng, Y., Gao, C., Wu, Y., Ma, J., He, R., Li, Q., Westin, C.F., Deslauriers-Gauthier, S., González, J.O.O., Paquette, M., St-Jean, S., Girard, G., Rheault, F., Sidhu, J., Tax, C.M.W., Guo, F., Mesri, H.Y., Dávid, S., Froeling, M., Heemskerk, A.M., Leemans, A., Boré, A., Pinsard, B., Bedetti, C., Desrosiers, M., Brambati, S., Doyon, J., Sarica, A., Vasta, R., Cerasa, A., Quattrone, A., Yeatman, J., Khan, A.R., Hodges, W., Alexander, S., Romascano, D., Barakovic, M., Auría, A., Esteban, O., Lemkaddem, A., Thiran, J.P., Cetingul, H.E., Odry, B.L., Mailhe, B., Nadar, M.S., Pizzagalli, F., Prasad, G., Villalon-Reina, J.E., Galvis, J., Thompson, P.M., Requejo, F.D.S., Laguna, P.L., Lacerda, L.M., Barrett, R., Dell'Acqua, F., Catani, M., Petit, L., Caruyer, E., Daducci, A., Dyrby, T.B., Holland-Letz, T., Hilgetag, C.C., Stieltjes, B., Descoteaux, M., 2017b. The challenge of mapping the human connectome based on diffusion tractography. Nat. Commun. 8, 1349. doi:10.1038/s41467-017-01285-x.
Maier-Hein, L., Eisenmann, M., Reinke, A., Onogur, S., Stankovic, M., Scholz, P., Arbel, T., Bogunovic, H., Bradley, A.P., Carass, A., Feldmann, C., Frangi, A.F., Full, P.M., van Ginneken, B., Hanbury, A., Honauer, K., Kozubek, M., Landman, B.A., März, K., Maier, O., Maier-Hein, K., Menze, B.H., Müller, H., Neher, P.F., Niessen, W., Rajpoot, N., Sharp, G.C., Sirinukunwattana, K., Speidel, S., Stock, C., Stoyanov, D., Taha, A.A., van der Sommen, F., Wang, C.W., Weber, M.A., Zheng, G., Jannin, P., Kopp-Schneider, A., 2018. Why rankings of biomedical image analysis competitions should be interpreted with care. Nat. Commun. 9, 5217. doi:10.1038/s41467-018-07619-7.
Miller, K.L., Alfaro-Almagro, F., Bangerter, N.K., Thomas, D.L., Yacoub, E., Xu, J., Bartsch, A.J., Jbabdi, S., Sotiropoulos, S.N., Andersson, J.L.R., Griffanti, L., Douaud, G., Okell, T.W., Weale, P., Dragonu, I., Garratt, S., Hudson, S., Collins, R., Jenkinson, M., Matthews, P.M., Smith, S.M., 2016. Multimodal population brain imaging in the UK Biobank prospective epidemiological study. Nat. Neurosci. 19, 1523–1536. doi:10.1038/nn.4393.
Mori, S., Frederiksen, K., van Zijl, P.C.M., Stieltjes, B., Kraut, M.A., Solaiyappan, M., Pomper, M.G., 2002. Brain white matter anatomy of tumor patients evaluated with diffusion tensor imaging. Ann. Neurol. 51, 377–380. doi:10.1002/ana.10137.
Moussavi-Biugui, A., Stieltjes, B., Fritzsche, K., Semmler, W., Laun, F.B., 2011a. Novel spherical phantoms for Q-ball imaging under *in vivo* conditions. Magn. Reson. Med. 65, 190–194. doi:10.1002/mrm.22602.
Moussavi-Biugui, A., Stieltjes, B., Fritzsche, K., Semmler, W., Laun, F.B., 2011b. Novel spherical phantoms for Q-ball imaging under *in vivo* conditions. Magn. Reson. Med. 65, 190–194.
Mushtaha, F.N., Kuehn, T.K., El-Deeb, O., Rohani, S.A., Helpard, L.W., Moore, J., Ladak, H., Moehring, A., Baron, C.A., Khan, A.R., 2021. Design and characterization of a 3D-printed axon-mimetic phantom for diffusion MRI. Magn. Reson. Med. doi:10.1002/mrm.28886, n/a.
Neher, P., Maier-Hein, K., 2020a. Simulated MRI Images and Reference Fiber Tracts of 99 subjects. (No. DKFZ-2020-01042). German Cancer Research Center doi:10.6097/e230-20200511_1.
Neher, P., Maier-Hein, K., 2020b. Sample data of the 99 simulated brains dataset. 10.5281/zenodo.4139626
Neher, P.F., Côté, M.A., Houde, J.C., Descoteaux, M., Maier-Hein, K.H., 2017a. Fiber tractography using machine learning. Neuroimage 158, 417–429. doi:10.1016/j.neuroimage.2017.07.028.
Neher, P.F., Descoteaux, M., Houde, J.C., Stieltjes, B., Maier-Hein, K.H., 2015. Strengths and weaknesses of state of the art fiber tractography pipelines – a comprehensive in-vivo and phantom evaluation study using Tractometer. Med. Image Anal. 26, 287–305. doi:10.1016/j.media.2015.10.011.
Neher, P.F., Houde, J.C., Descoteaux, M., Maier-Hein, K., 2017b. Tractography challenge ISMRM 2015 b=3000s/mm2 data. 10.5281/zenodo.1007149
Neher, P.F., Laun, F.B., Stieltjes, B., Maier-Hein, K.H., 2014. Fiberfox: facilitating the creation of realistic white matter software phantoms. Magn. Reson. Med. 72, 1460–1470. doi:10.1002/mrm.25045.
Neher, P.F., Maier-Hein, K.H., 2019. Simulated dMRI images and ground truth of random fiber phantoms in various configurations. 10.5281/zenodo.2533250
Neher, P.F., Maier-Hein, K.H., 2021. Providing realistic ground truth and AI-ready data for fiber tractography: the 99 simulated brains dataset. In: Proceedings of Annual Meeting ISMRM.
Newton, J.M., Ward, N.S., Parker, G.J.M., Deichmann, R., Alexander, D.C., Friston, K.J., Frackowiak, R.S.J., 2006. Non-invasive mapping of corticofugal fibres from multiple motor areas—relevance to stroke recovery. Brain J. Neurol. 129, 1844–1858. doi:10.1093/brain/awl106.
Nielsen, J.S., Sierra, A., Belevich, I., Jokitalo, E., Aggarwal, M., 2021. Exploring the epileptic rat hippocampus using oscillating gradients, 3D electron microscopy and Monte Carlo simulations. [WWW Document]. Proc. Int. Soc. Magn. Reson. Med. URL (accessed 7.23.21.
Palombo, M., Alexander, D.C., Zhang, H., 2019. A generative model of realistic brain cells with application to numerical simulation of the diffusion-weighted MR signal. Neuroimage 188, 391–402. doi:10.1016/j.neuroimage.2018.12.025.
Pan, D., Schmieder, A.H., Wickline, S.A., Lanza, G.M., 2011. Manganese-based MRI contrast agents: past, present and future. Tetrahedron 67, 8431–8444. doi:10.1016/j.tet.2011.07.076.
Panagiotaki, E., Schneider, T., Siow, B., Hall, M.G., Lythgoe, M.F., Alexander, D.C., 2012. Compartment models of the diffusion MR signal in brain white matter: a taxonomy and comparison. Neuroimage 59, 2241–2254.
Perrone, D., Aelterman, J., Pižurica, A., Jeurissen, B., Philips, W., Leemans, A., 2015. The effect of Gibbs ringing artifacts on measures derived from diffusion MRI. Neuroimage 120, 441–455. doi:10.1016/j.neuroimage.2015.06.068.
Perrone, D., Jeurissen, B., Aelterman, J., Roine, T., Sijbers, J., Pizurica, A., Leemans, A., Philips, W., 2016. D-BRAIN: anatomically accurate simulated diffusion MRI brain data. PLoS ONE 11, e0149778. doi:10.1371/journal.pone.0149778.
Poulin, P., Côté, M.A., Houde, J.C., Petit, L., Neher, P.F., Maier-Hein, K.H., Larochelle, H., Descoteaux, M., 2017. Learn to track: deep learning for tractography. In: Presented at the International Conference on Medical Image Computing and Computer-Assisted Intervention, MICCAI. Springer, Cham, pp. 540–547. doi:10.1007/978-3-319-66182-7_62 Lecture Notes in Computer Science.

Poupon, C., Rieul, B., Kezele, I., Perrin, M., Poupon, F., Mangin, J.F., 2008. New diffusion phantoms dedicated to the study and validation of high-angular-resolution diffusion imaging (HARDI) models. Magn. Reson. Med. 60, 1276–1283. doi:10.1002/mrm.21789.

Powell, H.W.R., Parker, G.J.M., Alexander, D.C., Symms, M.R., Boulby, P.A., Wheeler-Kingshott, C.A.M., Barker, G.J., Noppeney, U., Koepp, M.J., Duncan, J.S., 2006. Hemispheric asymmetries in language-related pathways: a combined functional MRI and tractography study. Neuroimage 32, 388–399. doi:10.1016/j.neuroimage.2006.03.011.

Pullens, P., Roebroeck, A., Goebel, R., 2010. Ground truth hardware phantoms for validation of diffusion-weighted MRI applications. J. Magn. Reson. Imaging 32, 482–488. doi:10.1002/jmri.22243.

Rafael-Patino, J., Romascano, D., Ramirez-Manzanares, A., Canales-Rodríguez, E.J., Girard, G., Thiran, J.P., 2020. Robust Monte-Carlo simulations in diffusion-MRI: effect of the substrate complexity and parameter choice on the reproducibility of results. Front. Neuroinformatics 0. doi:10.3389/fninf.2020.00008.

Reinke, A., Eisenmann, M., Onogur, S., Stankovic, M., Scholz, P., Full, P.M., Bogunovic, H., Landman, B.A., Maier, O., Menze, B., Sharp, G.C., Sirinukunwattana, K., Speidel, S., van der Sommen, F., Zheng, G., Müller, H., Kozubek, M., Arbel, T., Bradley, A.P., Jannin, P., Kopp-Schneider, A., Maier-Hein, L., 2018. How to exploit weaknesses in biomedical challenge design and organization. In: Frangi, A.F., Schnabel, J.A., Davatzikos, C., Alberola-López, C., Fichtinger, G. (Eds.), Medical Image Computing and Computer Assisted Intervention – MICCAI 2018, Lecture Notes in Computer Science. Springer International Publishing, Cham, pp. 388–395. doi:10.1007/978-3-030-00937-3_45.

Reischauer, C., Staempfli, P., Jaermann, T., Boesiger, P., 2009. Construction of a temperature-controlled diffusion phantom for quality control of diffusion measurements. J. Magn. Reson. Imaging 29 (3), 692–698. doi:10.1016/j.neuroimage.2008.05.002, : An Official Journal of the International Society for Magnetic Resonance in Medicine.

Reisert, M., Mader, I., Anastasopoulos, C., Weigel, M., Schnell, S., Kiselev, V., 2011. Global fiber reconstruction becomes practical. Neuroimage 54, 955–962. doi:10.1016/j.neuroimage.2010.09.016.

Reuter, J.A., Matuschke, F., Menzel, M., Schubert, N., Ginsburger, K., Poupon, C., Amunts, K., Axer, M., 2019. FAConstructor: an interactive tool for geometric modeling of nerve fiber architectures in the brain. Int. J. Comput. Assist. Radiol. Surg. 14, 1881–1889. doi:10.1007/s11548-019-02053-6.

Sarwar, T., Ramamohanarao, K., Zalesky, A., 2019. Mapping connectomes with diffusion MRI: deterministic or probabilistic tractography? Magn. Reson. Med. 81, 1368–1384. doi:10.1002/mrm.27471.

Sarwar, T., Seguin, C., Ramamohanarao, K., Zalesky, A., 2020. Towards deep learning for connectome mapping: a block decomposition framework. Neuroimage 212, 116654. doi:10.1016/j.neuroimage.2020.116654.

Schilling, K.G., Daducci, A., Maier-Hein, K., Poupon, C., Houde, J.C., Nath, V., Anderson, A.W., Landman, B.A., Descoteaux, M., 2019. Challenges in diffusion MRI tractography - lessons learned from international benchmark competitions. Magn. Reson. Imaging 57, 194–209. doi:10.1016/j.mri.2018.11.014.

Shaw, R., Sudre, C.H., Varsavsky, T., Ourselin, S., Cardoso, M.J., 2020. A k-space model of movement artefacts: application to segmentation augmentation and artefact removal. IEEE Trans. Med. Imaging 39, 2881–2892. doi:10.1109/TMI.2020.2972547.

Skudlarski, P., Jagannathan, K., Calhoun, V.D., Hampson, M., Skudlarska, B.A., Pearlson, G., 2008. Measuring brain connectivity: diffusion tensor imaging validates resting state temporal correlations. Neuroimage 43, 554–561. doi:10.1016/j.neuroimage.2008.07.063.

Staempfli, P., Jaermann, T., Crelier, G.R., Kollias, S., Valavanis, A., Boesiger, P., 2006. Resolving fiber crossing using advanced fast marching tractography based on diffusion tensor imaging. Neuroimage 30, 110–120.

Stieltjes, B., Kaufmann, W., van zijl, P., Fredericksen, K., Pearlson, G., Solaiyappan, M., Mori, S., 2001. Diffusion tensor imaging and axonal tracking in the human brainstem. Neuroimage 14, 723–735. doi:10.1006/nimg.2001.0861.

Tamnes, C.K., Roalf, D.R., Goddings, A.L., Lebel, C., 2018. Diffusion MRI of white matter microstructure development in childhood and adolescence: methods, challenges and progress. Dev. Cogn. Neurosci. 33, 161–175. doi:10.1016/j.dcn.2017.12.002, Methodological challenges in developmental neuroimaging: contemporary approaches and solutions.

Teem, n.d. tend helix 2021.

Théberge, A., Desrosiers, C., Descoteaux, M., Jodoin, P.M., 2020. Track-To-Learn: a general framework for tractography with deep reinforcement learning. bioRxiv 2020.11.16.385229. 10.1101/2020.11.16.385229

Tournier, J.D., Calamante, F., King, M., Gadian, D., Connelly, A., 2002. Limitations and requirements of diffusion tensor fiber tracking: an assessment using simulations. Magn. Reson. Med. 47, 701–708.

Tournier, J.D., Mori, S., Leemans, A., 2011. Diffusion tensor imaging and beyond. Magn. Reson. Med. 65, 1532–1556. doi:10.1002/mrm.22924.

Tournier, J.D., Yeh, C.H., Calamante, F., Cho, K.H., Connelly, A., Lin, C.P., 2008. Resolving crossing fibres using constrained spherical deconvolution: validation using diffusion-weighted imaging phantom data. Neuroimage 42, 617–625. doi:10.1016/j.neuroimage.2008.05.002.

van den Heuvel, M.P., de Reus, M.A., Barrett, L.F., Scholtens, L.H., Coopmans, F.M.T., Schmidt, R., Preuss, T.M., Rilling, J.K., Li, L., 2015. Comparison of diffusion tractography and tract-tracing measures of connectivity strength in rhesus macaque connectome. Hum. Brain Mapp. 36, 3064–3075. doi:10.1002/hbm.22828.

Van Essen, D.C., Ugurbil, K., Auerbach, E., Barch, D., Behrens, T.E.J., Bucholz, R., Chang, A., Chen, L., Corbetta, M., Curtiss, S.W., Della Penna, S., Feinberg, D., Glasser, M.F., Harel, N., Heath, A.C., Larson-Prior, L., Marcus, D., Michalareas, G., Moeller, S., Oostenveld, R., Petersen, S.E., Prior, F., Schlaggar, B.L., Smith, S.M., Snyder, A.Z., Xu, J., Yacoub, E., 2012. The human connectome project: a data acquisition perspective. NeuroImage 62, 2222–2231. doi:10.1016/j.neuroimage.2012.02.018, Connectivity.

Von dem Hagen, E.A., Henkelman, R.M., 2002. Orientational diffusion reflects fiber structure within a voxel. Magn. Reson. Med. 48 (3), 454–459 An Official Journal of the International Society for Magnetic Resonance in Medicine.

Wasserthal, J., Neher, P., Maier-Hein, K.H., 2018. TractSeg - fast and accurate white matter tract segmentation. Neuroimage 183, 239–253.

Wegmayr, V., Giuliari, G., Buhmann, J.M., 2019. Entrack: a data-driven maximum-entropy approach to fiber tractography. In: Fink, G.A., Frintrop, S., Jiang, X. (Eds.), Pattern Recognition, Lecture Notes in Computer Science. Springer International Publishing, Cham, pp. 232–244. doi:10.1007/978-3-030-33676-9_16.

Wu, X., Xie, M., Zhou, J., Anderson, A.W., Gore, J.C., Ding, Z., 2012. Globally optimized fiber tracking and hierarchical clustering - a unified framework. Magn. Reson. Imaging 30, 485–495.

Wu, Y., Sun, D., Wang, Yong, Wang, Yunjie, Wang, Yibao, 2016. Tracing short connections of the temporo-parieto-occipital region in the human brain using diffusion spectrum imaging and fiber dissection. Brain Res. 1646, 152–159. doi:10.1016/j.brainres.2016.05.046.

Ye, A.Q., Cristinacce, P.L.H., Zhou, F.L., Yin, Z., Parker, G.J.M., Magin, R.L., 2014. Diffusion tensor MRI phantom exhibits anomalous diffusion. In: Proceedings of the 36th Annual International Conference of the IEEE Engineering in Medicine and Biology Society, pp. 746–749. doi:10.1109/EMBC.2014.6943698.

Zalesky, A., Fornito, A., Seal, M.L., Cocchi, L., Westin, C.F., Bullmore, E.T., Egan, G.F., Pantelis, C., 2011. Disrupted axonal fiber connectivity in schizophrenia. Biol. Psychiatry 69, 80–89. doi:10.1016/j.biopsych.2010.08.022.

Zemmoura, I., Serres, B., Andersson, F., Barantin, L., Tauber, C., Filipiak, I., Cottier, J.P., Venturini, G., Destrieux, C., 2014. FIBRASCAN: a novel method for 3D white matter tract reconstruction in MR space from cadaveric dissection. Neuroimage 103, 106–118. doi:10.1016/j.neuroimage.2014.09.016.

Zhan, L., Zhou, J., Wang, Y., Jin, Y., Jahanshad, N., Prasad, G., Nir, T.M., Leonardo, C.D., Ye, J., Thompson, P.M.for the Alzheimer's Disease Neuroimaging Initiative, 2015. Comparison of nine tractography algorithms for detecting abnormal structural brain networks in Alzheimer's disease. Front. Aging Neurosci. 7. doi:10.3389/fnagi.2015.00048.

Zhang, H., Schneider, T., Wheeler-Kingshott, C.A., Alexander, D.C., 2012. NODDI: practical in vivo neurite orientation dispersion and density imaging of the human brain. Neuroimage 61, 1000–1016.

Zhang, Z., Johnson, D.L., Schwartz, L.M., 2011. Simulating the time-dependent diffusion coefficient in mixed-pore-size materials. Phys. Rev. E 84, 031129.

Zhou, F.L., Hubbard, P.L., Eichhorn, S.J., Parker, G.J.M., 2012. Coaxially electrospun axon-mimicking fibers for diffusion magnetic resonance imaging. ACS Appl. Mater. Interfaces 4, 6311–6316. doi:10.1021/am301919s.

Zhou, F.L., Li, Z., Gough, J.E., Hubbard Cristinacce, P.L., Parker, G.J.M., 2018. Axon mimicking hydrophilic hollow polycaprolactone microfibres for diffusion magnetic resonance imaging. Mater. Des. 137, 394–403. doi:10.1016/j.matdes.2017.10.047.

Zhou, F.L., McHugh, D.J., Li, Z., Gough, J.E., Williams, G.R., Parker, G.J.M., 2021. Coaxial electrospun biomimetic copolymer fibres for application in diffusion magnetic resonance imaging. Bioinspir. Biomim. 16, 046016. doi:10.1088/1748-3190/abedcf.